

1 Design and validation of MEDRYS, a Mediterranean Sea 2 reanalysis over 1992-2013

3
4 **M. Hamon¹, J. Beuvier^{1,2}, S. Somot², J.M. Lellouche¹, E. Greiner³, G. Jordà⁴,**
5 **M.N. Bouin², T. Arsouze⁵, K. Béranger⁶, F. Sevault², C. Dubois¹, M. Drevillon¹**
6 **and Y. Drillet¹.**

7 [1]{Mercator Océan, 10 rue Hermès, 31520 Ramonville-Saint-Agne, France}

8 [2]{Météo France, 42 av. Gaspard Coriolis, 31057 Toulouse cedex, France}

9 [3] {CLS, 11 rue Hermès, 31520 Ramonville-Saint-Agne, France }

10 [4] {Department of Ecology and Marine Resources, IMEDEA (CSIC-UIB), Institut
11 Mediterrani d'Estudis Avançats, Esporles (Illes Balears), Spain}

12 [5] {LMD, école Polytechnique, 91128 Palaiseau cedex, France}

13 [6] {LTHE, rue de la Piscine, 38400 Saint-Martin d'Hère, France}

14 Correspondence to: J. Beuvier (jonathan.beuvier@mercator-ocean.fr)

16 Abstract

17
18 The French research community on the Mediterranean Sea modelling and the French
19 operational ocean forecasting center Mercator Océan have gathered their skill and expertise in
20 physical oceanography, ocean modelling, atmospheric forcings and data assimilation, to carry
21 out a MEDiterranean sea ReanalYsis (MEDRYS) at high resolution for the period 1992-
22 2013. The ocean model used is NEMOMED12, a Mediterranean configuration of NEMO with
23 a $1/12^\circ$ (~ 7 km) horizontal resolution and 75 vertical z-levels with partial steps. At the
24 surface, it is forced by a new atmospheric forcing dataset (ALDERA), coming from a
25 dynamical downscaling of the ERA-Interim atmospheric reanalysis by the regional climate
26 model ALADIN-Climate with a 12-km horizontal and 3-hour temporal resolutions. This
27 configuration is used to carry a 34-year hindcast simulation over the period 1979-2013
28 (NM12-FREE) which is the initial state of the reanalysis in October 1992. MEDRYS uses the

1 existing Mercator Océan data assimilation system SAM2 that is based on a reduced-order
2 Kalman filter with a 3D multivariate modal decomposition of the forecast error. Altimeter
3 data, satellite SST and temperature and salinity vertical profiles are jointly assimilated. This
4 paper describes the configuration we used to perform MEDRYS. We then validate the skills
5 of the data assimilation system. It is shown that the data assimilation restores a good averaged
6 temperature and salinity at intermediate layers compared to the hindcast. No particular biases
7 are identified in the bottom layers. However, the reanalysis show slight positive biases of
8 0.02psu and 0.15°C above 150m depth. In the validation stage, it is also shown that the
9 assimilation allows to better reproduce water, heat and salt transports through the Strait of
10 Gibraltar. Finally, the ability of the reanalysis to represent the sea surface high frequency
11 variability is pointed out.

12

13 **1. Introduction**

14

15 The Mediterranean Sea is a semi-enclosed sea located between 5.5°W and 36°E and
16 between 30°N and 46°N. It is connected to the Atlantic Ocean through the Strait of Gibraltar
17 and to the Black Sea through the Dardanelles and the Bosphorus Straits. The surrounding
18 orography tends to generate cold and dry regional northern winds over the Mediterranean Sea.
19 This leads to strong heat and freshwater losses by evaporation and latent heat transfer. The
20 heat loss is estimated around 5 W/m² (MacDonald et al., 1994) while the freshwater loss is
21 about 0.6 m/yr (Mariotti et al., 2008). The main part of the heat and water atmospheric losses
22 are balanced by warm Atlantic Waters (AW) entering through the Strait of Gibraltar while it
23 is estimated that only about 10% of the net water flux is balanced with river runoff (Struglia
24 et al., 2004).

25

26 In a climate change context, the Mediterranean area is considered as a hot spot and shows an
27 increase in the temperature and precipitation interannual variability, and a strong warming and
28 drying (Giorgi et al., 2006). The vulnerability of the population is likely to increase with a
29 higher probability of occurrence of events leading to floods and droughts, which are among
30 the most devastating natural hazards. In this context, it is necessary to simulate the water
31 cycle over the Mediterranean basin (Drobinski et al., 2013) and to understand how it will

1 impact water resources. We must improve our understanding of the variability of the water
2 cycle, from extreme events to the seasonal and interannual scales. In addition to the socio-
3 economic motivations and from a strictly physical point of view, the specific configuration of
4 the basin also permits the study of a wide variety of dynamical oceanic processes. For
5 example, the Mediterranean Sea has been found to have a dominant mesoscale circulation
6 component (Robinson et al., 1987; Ayoub et al., 1998; Hamad et al., 2005; Fernandez et al.,
7 2005) in addition to a thermohaline circulation similar to the world ocean (Wüst, 1961;
8 Robinson et al., 2001). The Mediterranean eddy field also shows semi-permanent structures
9 (Rhodes and South Adriatic gyres for example) that define the general circulation in the
10 basin. Modeling the different time and spatial scales of this circulation is still challenging
11 because for example of approximations and uncertainties on non-linear dynamical balance,
12 atmospheric forcing or the bathymetry (Sorgente et al., 2011; Pinardi et al., 2013).

13

14 The ocean reanalysis is a reconstruction technique that allows the production of a consistent
15 four-dimensional estimate of a physical field from observations and numerical modeling
16 simulation. Observations are used to constrain the model trajectory to be as close as possible
17 to the “real” state of the ocean. Ocean reanalyses are thus reference products which help to
18 improve our knowledge of the ocean variability at various space and time scales. Several
19 techniques have been used in the past to produce large-scale reanalysis but regional reanalysis
20 are challenging because observational datasets are scarcer and the use of high resolution
21 model requires to adequately represent fluxes through the air/sea interface. This is even more
22 important in the Mediterranean Sea due to the complex orography. Many small-size islands
23 and a particularly complex coastline limit the low-level air flow, channeling potentially strong
24 and recurring regional winds (Mistral, Tramontane, Bora, Etesian, Sirocco; Herrmann et al.,
25 2011). The role of the spatial resolution of the forcing has been highlighted as a key aspect of
26 the representation of Mediterranean Sea phenomena such as local winds (Sotillo et al., 2005 ;
27 Ruti et al., 2007 ; Herrmann et al., 2011 ; Lebeaupin Brossier et al., 2012), open-sea deep
28 convection (Herrmann and Somot, 2008 ; Béranger et al., 2010), shelf-cascading (Dufau-
29 Jullian et al., 2004; Langlais et al., 2009), coastal upwelling (Estournel et al., 2009; Casella
30 et al., 2011), permanent circulation features (Estournel et al., 2003; Ourmières et al., 2011) or
31 intermittent eddies (Marullo et al., 2003; Ciappa, 2009; Rubio et al., 2009). The infra-diurnal
32 temporal resolution of the forcing has also been identified as necessary to represent key

1 phenomena such as large salinity anomalies following intense rainfall events (Lebeaupin
2 Brossier et al., 2012) or the SST diurnal cycle (Lebeaupin Brossier et al., 2011, 2014). Other
3 studies demonstrated the importance of the good representation of the atmospheric synoptic
4 chronology linked with the so-called weather patterns or weather regimes (Josey et al., 2011 ;
5 Papadopoulos et al., 2012 ; Durrieu de Madron et al., 2013) or with the passage of
6 Mediterranean storms associated with strong air-sea exchanges (Herrmann and Somot, 2008 ;
7 Herrmann et al., 2010). At a longer time scale, interannual to decadal variability of the
8 atmospheric forcings (water or heat fluxes) is known to dominate the climate variability of the
9 deep water mass formation in both basins of the Mediterranean Sea (Beuvier et al. 2010;
10 Herrmann et al. 2010; L'Heveder et al., 2013) leading sometimes to exceptionnal decadal
11 events such as the Eastern Mediterranean Transient (Roether et al., 2007) or the Western
12 Mediterranean Transition (Schroeder et al., 2008).

13

14 The first regional Mediterranean reanalyses have been recently produced over the 1985-2007
15 period by Adani et al. (2011), using a reduced-order optimal interpolation and a three-
16 dimensional variational scheme. Their OPA ocean model (Madec et al., 1997) on a $1/16^\circ$
17 regular horizontal grid (Tonani et al., 2008) is forced by daily atmospheric fields from the
18 European Center Medium-Range Weather Forecast (ECMWF) with bulk parameterizations
19 and a monthly precipitation climatology. They used the reanalysis ERA-15 for the 1985-1992
20 period and then the operational analyses for the 1993-2007 period. We note thus several
21 successive changes in the atmospheric forcing, in particular during the 1993-2007 period, for
22 which the resolution of the ECMWF analyses has progressively increased in several steps
23 from about 100km to 25km. Such changes suggest that temporal continuity and coherence in
24 atmospheric forcing are not guaranteed. However, the first results of these reanalyses pointed
25 out for example that such products allow to better simulate the AW salinity inflow, the sea
26 surface height variability, and current-jet pathways.

27

28 In the same way of these previous studies and in order to enhance the diversity of the
29 Mediterranean Sea reanalyses, we present in this study another reanalysis of the
30 Mediterranean circulation, MEDRYS, performed with different tools and covering the
31 altimetry 1992-2013 period. Our ocean model used is NEMOMED12 (Beuvier et al., 2012a),
32 a Mediterranean configuration of NEMO (Madec and the NEMO team, 2008; an update

1 version of the OPA code) with the ORCA12 standard grid. The ORCA12 grid shows a
2 varying resolution around $1/12^\circ$ over the world ocean. Within our numerical domain, the
3 ORCA grid has a horizontal resolution ranging between 6 and 7.5km. Note that this spatial
4 resolution is similar is to the $1/16^\circ$ regular horizontal grid used in Adani et al. (2011).
5 MEDRYS differs also by the use of a reduced-order Kalman filter in the assimilation scheme
6 from the French operational oceanography center Mercator Océan and the long-term 12-km
7 high-resolution fields of the atmospheric forcing called ALDERA. Even if we cannot
8 overcome other homogeneity issues resulting from the coverage of the observing network
9 (applying in both MEDRYS and ALDERA), we pay a special attention to the consistency of
10 the atmospheric forcing (same resolution, same model physics) in order to reduce as most as
11 possible the sources of inhomogeneity in MEDRYS. This reanalysis then contributes to better
12 describe the interannual to decadal variability of the Mediterranean circulation and trends

13

14 In the current paper, we first present the configuration of the reanalysis MEDRYS and the
15 twin hindcast NM12-FREE in section 2. Then, section 3 presents validation diagnostics and
16 some scientific assessments. Finally, discussions and conclusion are conducted in section 4.

17

18 **2. Experimental set up**

19

20 Two twin simulations have been produced: MEDRYS, a Mediterranean reanalysis
21 covering the 1992-2013 period with data assimilation and its associated free run NM12-
22 FREE, a 34-year hindcast simulation covering the 1979-2013 period without assimilation.
23 Both simulations use the same ocean model configuration, NEMOMED12, described in
24 sections 2.1 and the high resolution atmospheric forcing ALDERA, presented in section 2.3.
25 Specific set up concerning data assimilation in the reanalysis are then presented in sections
26 2.4 and 2.5.

27

28 **2.1 Ocean model configuration : NEMOMED12**

29

1 We use the ocean general circulation model NEMO (Madec and the NEMO team, 2008)
2 in a regional configuration of the Mediterranean Sea called NEMOMED12 (Lebeaupin
3 Brossier et al., 2011, 2012, Beuvier et al., 2012a and 2012b ; hereafter NM12). The
4 development of NM12 is made in the continuity of the evolution of the French modeling of
5 the Mediterranean Sea, following OPAMED16 (Beranger et al., 2005), OPAMED8 (Somot et
6 al., 2006) and NEMOMED8 (Beuvier et al., 2010). More details concerning the physical
7 parametrizations and the boundary conditions in NM12 can be found in Beuvier et al.
8 (2012a).

9

10 The NM12 configuration covers the whole Mediterranean Sea and a buffer zone including a
11 part of the Atlantic basin, but not the Black Sea. The horizontal resolution is $1/12^\circ$ and
12 corresponds to a varying grid cell size between 6 and 7.5km (the distance between two points
13 varying with the cosine of the latitude). NM12 has 75 vertical stretched z-levels (from Δz
14 =1m at the surface to $\Delta z = 135\text{m}$ at the bottom, with 43 levels in the first 1000m) in a partial
15 step configuration. The bottom layer thickness is varying to fit the bathymetry (Mercator-
16 LEGOS version 10 bathymetry at $1/120^\circ$ resolution). The no-slip boundary condition is used
17 and the conservation of the model volume is assumed. The mean tidal effect of the quadratic
18 bottom friction formulation computed from a tidal model (Lyard et al., 2006) has been taken
19 into account leading to significant additional bottom friction in the Strait of Gibraltar,
20 Channel of Sicily, Gulf of Gabes and the northern Adriatic sub-basin. As a lateral boundary
21 conditions and in order to represent the exchanges with the Atlantic ocean, a buffer zone is
22 used: from 11° to 7.5°W , 3D temperature and salinity, as well as the Sea Surface Height
23 (SSH) fields are relaxed toward ORAS4 global ocean reanalysis monthly fields (Balmaseda et
24 al. 2013), produced by the European Centre for Medium Range Weather Forecast (ECMWF).
25 For temperature and salinity, the restoring term in the buffer zone is weak west of Cadiz and
26 Gibraltar areas and increases westwards. As the Mediterranean Sea is an evaporation basin,
27 the model volume is conserved through the damping of the SSH in the buffer zone toward
28 prescribed SSH anomalies with a very strong restoring. The SSH from ORAS4 is set in the
29 Atlantic according to a strong damping with a very small characteristic time-scale ($\tau = 2\text{ s}$).

30

31 We use the climatological averages of the interannual dataset of Ludwig et al. (2009) to
32 compute monthly runoff values, split in two parts (Beuvier et al., 2012a). The 33 main rivers

1 of the NM12 domain are added as precipitation at mouth points (29 in the Mediterranean Sea
2 and 4 in the buffer zone). As the Ludwig et al. (2009) dataset consists in 239 mouth points,
3 the inputs of the 210 other rivers in the Mediterranean basin are gathered as a coastal runoff in
4 each subbasin (following the same dividing as in Ludwig et al. 2009). Until 2000, we use the
5 interannual values from Ludwig et al. (2009) and then the climatological average representing
6 the 1960-2000 period. The Black Sea, not included NM12, is taken into account with a
7 monthly average one layer net flow across the Marmara Sea and the Dardanelles Strait. We
8 assume that the flow is a freshwater flux (Beuvier et al., 2012a). Until 1997, we use the
9 interannual values from Stanev et Peneva (2002) and then the climatological average
10 representing the 1960-1997 period.

11

12 **2.2 Simulations: NM12-FREE and MEDRYS**

13

14 The hindcast NM12-FREE starts in October 1979 and ends in June 2013. In the
15 Mediterranean side, initial conditions are provided by a monthly mean potential temperature
16 and salinity 3-D fields based on the MedAtlas interannual dataset (Rixen et al., 2005). A field
17 representing the state of the Mediterranean Sea in October 1979 has been produced
18 combining the MedAtlas monthly climatology (MEDAR/MEDATLAS Group, 2002) to the 3-
19 year filtered interannual fields from Rixen et al. (2005). Following Rixen et al. (2005), the
20 filtered interannual product is used in order to reduce the impact of large spatio-temporal gaps
21 in the data distribution. In the buffer zone, potential temperature and salinity are initialized
22 from ORAS4 global ocean reanalysis fields in order to maintain consistency with the
23 relaxation. In the initial condition fields, a linear transition between 7.5°W and 6°W is applied
24 between the ORAS4 and the MedAtlas fields. MEDRYS starts from the state of NM12-FREE
25 in October 1992 and ends in June 2013.

26

27 **2.3 Atmospheric forcing: ALDERA**

28

29 The most recent long-term hindcast simulations using the NEMOMED12 ocean model
30 (Beuvier et al. 2012B; Soto-Navarro et al. 2014; Palmiéri et al. 2015) were driven by the
31 ARPERA2 dataset (Herrmann et al. 2010). This forcing was obtained by a dynamical

1 downscaling using the stretched-grid Regional Climate Model (RCM) ARPEGE-Climate and
2 a spectral nudging technique. ARPERA2 covers the period 1958-2013 with a daily temporal
3 resolution and a 50-km spatial resolution over the Mediterranean Sea. It may include
4 temporal inhomogeneity especially in 2001 when the large-scale driving fields changes from
5 ERA-40 to ECMWF analysis.

6 In order to overcome the main deficiencies of the ARPERA2 dataset (relatively coarse spatial
7 and temporal resolution, temporal homogeneity issue), we are using a new forcing dataset for
8 MEDRYS and NM12-FREE. This dataset (called hereafter ALDERA) is based on a
9 dynamical downscaling of the ERA-Interim reanalysis (Dee et al., 2011) over the period
10 1979–2013 by the RCM ALADIN-Climate (Radu et al., 2008; Colin et al., 2010; Herrmann et
11 al., 2011). The dynamical downscaling technique is commonly used to overcome the lack of
12 atmospheric regional reanalysis over sea and to improve locally the resolution of the air-sea
13 forcing in areas dominated by small-scale atmospheric pattern as the Mediterranean Sea
14 (Sotillo et al. 2005, Herrmann and Somot 2008, Beuvier et al. 2010, Herrmann et al. 2010,
15 Herrmann et al. 2011, Josey et al. 2011, Beuvier et al. 2012a, Lebeaupin-Brossier et al. 2012,
16 Solé et al. 2012, Vervatis et al. 2013, Auger et al. 2014, Harzallah et al. 2014). In ALDERA,
17 we use the version 5 of ALADIN-Climate firstly described in Colin et al. (2010). For the
18 model definition, we used a Lambert conformal projection for pan-Mediterranean area at the
19 horizontal resolution of 12 km centred at 14°E, 43°N with 405 grid points in longitude and
20 261 grid points in latitude excluding the coupling zone. The model version has 31 vertical
21 levels. The time step used is 600 seconds. This geographical set-up allows the Med-CORDEX
22 official area (Ruti et al. 2015 in revision, www.medcordex.eu) to be fully included in the
23 model central zone. In this configuration, the RCM is driven at its lateral boundary by the
24 ERA-Interim reanalysis (T255, 80-km at its full resolution, Dee et al., 2011,
25 <http://www.ecmwf.int/research/era/do/get/era-interim>) which are updated every 6 hours. The
26 ERA-Interim data assimilation system uses a 2006 release of the Integrated Forecasting
27 System, which contains many improvements both in the forecasting model and analysis
28 methodology relative to ERA-40. Before starting this simulation, a two-year long spin-up is
29 carried out allowing the land water content to reach its equilibrium. Land surface parameters
30 and aerosols concentration are updated every month following a climatological seasonal cycle
31 coming from observations. The sea surface temperatures and the sea ice limit are updated
32 every month with a seasonal and interannual variability using the same SST and sea ice
33 analyses as the one used to drive the ERA-Interim reanalysis (Dee et al 2011). As atmospheric

1 reanalyses constitutes today the best knowledge of the 4-D dynamic of the atmosphere
2 available over the last decades, such a simulation is often called “perfect-boundary
3 simulation” or “poor-man regional reanalysis”.

4

5 ALDERA is available at a 12-km spatial resolution and a 3-hour temporal resolution over the
6 whole Mediterranean Sea, Black Sea and near-Atlantic Ocean. It includes a representation of
7 the effect of the aerosols on the long-wave and short-wave radiations and uses the same bulk
8 formula as in ARPERA2 (Louis, 1979) to compute the turbulent fluxes (sensible heat, latent
9 heat and momentum fluxes). All variables required to drive regional ocean models using bulk
10 formula or flux formulation are available. For the NEMOMED12 configuration (both NM12-
11 FREE and MEDRYS), reanalysis, the various fluxes have been interpolated every 3-hour on
12 the NEMOMED12 grid using a conservative interpolation scheme. NEMOMED12 receives
13 heat fluxes (total and solar for the light penetration), net freshwater fluxes (evaporation and
14 precipitation) and wind stresses every 3 hours. A retroaction term towards the same SST
15 fields as the one seen by ALADIN-Climate is added in the heat flux, following the method of
16 Barnier et al. (1995), with a retroaction coefficient of $-40 \text{ W.m}^{-2}.\text{K}^{-1}$. The total heat flux,
17 including the retroaction term, has been stored when running the hindcast NM12-FREE and is
18 used to force MEDRYS, ensuring thus that both simulations have exactly the same
19 atmospheric forcing.

20

21 No SSS damping is used but a 2D-smoothed monthly climatological freshwater flux
22 correction is added, following the same method as in Beuvier et al. (2012a), but with the 2D
23 spatial variability kept : these monthly 2D fields have been computed by averaging the SSS
24 relaxation term through a previous companion simulation with NEMOMED12 and the same
25 atmospheric forcing, and then filtered at the resolution of 1° by a spatial averaging. The
26 surface freshwater budget is thus balanced without altering the spatial and temporal variations
27 of the freshwater flux and so of the SSS. This correction term is added to the water fluxes
28 coming from the atmospheric fields and from the rivers and Black Sea runoff.

29

30 Within the frame of the Med-CORDEX initiative, the RCM ALADIN-Climate is also run at
31 lower spatial resolutions (150km and 50km) with exactly the same setting as ALDERA in

1 order to illustrate the small-scale features of the 12km resolution model with respect to lower
2 resolution models (see later comments for Tables 1 and 2 and Figs. 1 and 2).

3 4 **2.3.1 Long-term Mediterranean Sea surface heat and water budgets**

5
6
7 Table 1 and 2 compares the spatially and temporally averaged values of the Mediterranean
8 Sea surface heat and water budget terms of the ALDERA forcing with past studies and
9 observed-based references (flux are positive downward in $\text{W}\cdot\text{m}^{-2}$ and mm/day). ALDERA
10 shows values within the range of the references for the net heat and water surface fluxes,
11 respectively with $-3 \text{ W}\cdot\text{m}^{-2}$ over the 1985-2004 period ($-4 \text{ W}\cdot\text{m}^{-2}$ over the 1979-2012 period)
12 and $-1.69 \text{ mm}\cdot\text{day}^{-1}$ (1979-2011). Over the 20-year period considered, ALDERA shows
13 compensating errors between an overestimated shortwave and an overestimated latent heat
14 loss when compared to the observation-based estimates (Sevault et al. 2014). Both values are
15 in equilibrium with the heat and water transports at the Strait of Gibraltar (see section 3.2.6).
16 However some individual terms show biases. This is especially true for the shortwave
17 radiation, the latent heat flux (and consequently the evaporation) and the precipitation
18 averaged over the sea surface. Note that ALDERA and ARPERA2 show very similar results,
19 what is expected as they share most of their physical parameterizations. This also means that
20 increasing the spatial resolution in the RCMs does not fundamentally change the mean biases
21 at least from 50km to 12km. This is confirmed when comparing ALDERA to the ALADIN-
22 Climate simulation at 50km resolution. ALADIN-Climate ran at 150 km is however closer to
23 ERA-Interim with a weaker latent heat loss. Note that Pettenuzzo et al. (2010) dataset also
24 achieves the Mediterranean sea heat budget balance but with lower values both for the
25 shortwave radiation and the latent heat loss. When compared to the ENSEMBLES RCMs
26 used in the last published multi-model intercomparison study with Atmosphere RCM
27 (Sanchez-Gomez et al. 2011), ALDERA always fits inside the uncertainty range.

28 29 **2.3.2 Interannual variability and trends**

1 At the basin scale, the interannual variability of the various terms of the Mediterranean
2 Sea heat budget can also be evaluated for the period 1985-2004 of the reference dataset of
3 Table 1 (Sevault et al. 2014). For example, for the basin-averaged net shortwave radiation
4 flux, the interannual standard deviation in ALDERA (1.6 W.m^{-2}) is underestimated with
5 respect to ISCCP observations (2.8 W.m^{-2}) whereas the interannual temporal correlation is
6 equal to 0.84. For the latent heat loss, the 1985-2004 interannual standard deviation is equal to
7 5.6 W.m^{-2} in ALDERA within the range of the observations (4.7 W.m^{-2} for NOCS and 6.7
8 W.m^{-2} for OAFLUX) and the interannual temporal correlation is good (0.83 with NOCS and
9 0.81 with OAFLUX). Interannual standard deviations are lower for the net longwave radiation
10 flux (1.2 W.m^{-2} in ALDERA) and for the sensible heat loss (1.3 W.m^{-2} in ALDERA) and the
11 various observation-based estimates disagree (not shown).

12
13 Trends in the surface forcing are relevant in long-term simulations as they can induce long-
14 term trends in the water mass characteristics. Concerning the surface heat flux terms in
15 ALDERA, only the trend in latent heat flux is significant with an increase in the heat loss by
16 the sea equal to $+4.1 \text{ W/m}^2/\text{decade}$ over the 1979–2012 period. This trend is similar to the one
17 obtained in Mariotti et al. (2008) and is mostly driven by the SST trends (Sevault et al. 2014).
18 Note that ALDERA does not include the observed trend in European anthropogenic aerosols
19 and therefore does not reproduce the shortwave trend identified in Nabat et al. (2014).

20

21 **2.3.3 Illustration of the small-scale features in the ALDERA forcing**

22

23 Over the Mediterranean Sea, the added-value of high-resolution models has been shown
24 in particular concerning the representation of the heat and water budget terms (Elguindi et al.
25 2011, Josey et al. 2011), of wind field especially close to the coast and islands (Sotillo et al.
26 2005, Ruti et al. 2007, Herrmann and Somot 2008, Langlais et al. 2009, Herrmann et al. 2011,
27 Vrac et al. 2012) and of the events of strong air-sea fluxes (Herrmann and Somot 2008,
28 Béranger et al. 2010, Lebeaupin-Brossier et al. 2012). Dynamical downscaling of reanalyses
29 have therefore been used to force long-term hindcast simulations (Beuquier et al. 2010, 2012,
30 Herrmann et al. 2010, Solé et al. 2012, Vervatis et al. 2013, Auger et al. 2014, Harzallah et al.
31 2014). Figure 1 illustrates the role of the atmospheric resolution in the representation of the

1 wind and the latent heat flux on March 14th 2013 in the Gulf of Lions by comparing
2 ALDERA at 12 km with ALADIN-Climate runs at lower-resolution. This particular date has
3 been selected because of the strong Mistral event in the Gulf of Lions. Increasing the
4 resolution allows ALDERA to create small-scale features of the wind near the coast as well as
5 the associated pattern of latent heat flux during the Mistral event. The comparison of latent
6 heat flux at 42°N, 5°E also indicates that the maximum of latent heat flux is resolution-
7 dependent. In ALADIN-12km (the so-called ALDERA), the maximum of latent heat loss is
8 about $900\text{W}\cdot\text{m}^{-2}$ whereas in ALADIN-150km, it barely reaches $500\text{W}\cdot\text{m}^{-2}$ with ALADIN-
9 50km being intermediate.

10

11 Figure 2 also illustrates the resolution dependency of the surface wind field but over the
12 Eastern Mediterranean basin during a Meltem (or Etesian) event (August 16th 2012). This
13 case shows the clear shadowing effect of the Greek islands. The wind channeling at 12 km
14 leads locally to increased wind speed, changes in wind direction and increased vorticity inputs
15 for the ocean due to strong horizontal gradients. All these effects are visible at the South-
16 Eastern part of Crete, an area where the Ierapetra anticyclone is formed regularly (see below).
17 Note that the goal here is not to prove the added value of the 12 km with respect to lower
18 resolution as in-situ observations and regridded would be required for this purpose but to
19 illustrate differences between the 3 resolutions (150, 50 and 12 km) and to show ALDERA
20 small-scale features with potential impacts on local to regional Mediterranean Sea circulation.

21

22 **2.4 Data assimilation scheme**

23

24 The data assimilation system used in MEDRYS is SAM2 (Système d'Assimilation
25 Mercator 2nd version), which is used at Mercator Océan for operational oceanography
26 purposes. The Mercator Océan monitoring and forecasting system has demonstrated its skills
27 for the global ocean forecast (Lellouche et al., 2013) and we used it in a regional
28 configuration. As the main part of the assimilation scheme used in this paper is already
29 described by Lellouche et al. (2013), we will summarize the assimilation methodology and
30 focus on the specifications inherent to the Mediterranean configuration.

31

1 The SAM2 data assimilation method relies on a reduced-order Kalman filter based on the
2 singular evolutive extended Kalman filter (SEEK) with a 7-day assimilation window
3 (hereafter referred as the assimilation cycle). For each assimilation cycle in MEDRYS, SAM2
4 produces increments of SSH, temperature, salinity and velocity (zonal and meridional
5 components) from the model and the observations, weighted by the forecast error covariance
6 and the specified observation error. Increments are then applied as a tendency term in the
7 model prognostic equations. The forecast error covariance is based on the statistics of a
8 collection of 3D ocean state anomalies. For a given cycle centred on the Nth day of a given
9 year, ocean state anomalies computed from NM12-FREE within the window [N – 60 days ; N
10 + 60 days] of each year are gathered and define the covariance of the model forecast error.
11 For the Mediterranean configuration, we computed about 900 anomaly fields from NM12-
12 FREE for a given assimilation cycle. Compared to a global configuration, the moderate size
13 of the domain allows us to use such a number of anomaly fields (about 300 in a global
14 configuration) in order to statically compute an accurate error covariance field. Moreover, as
15 the analysis increment is a linear combination of the anomalies, a large amount of anomalies
16 is desirable in order to better span the oceanic variability.

17

18

19 In the original formulation of SAM2, SSH increments are analytically computed from
20 temperature and salinity increments through barotropic/dynamic height balances (Lellouche et
21 al., 2013). This assumption is only valid far from the coast and in open seas, where the local
22 SSH variations due to the remote wind are negligible. In the Mediterranean Sea, strong
23 regional winds occur in areas with low bathymetry and near important straits like Gibraltar
24 and Sicily. A significant part of SSH is then driven non locally by the wind. Shelf surge and
25 hydraulic control effects are typically 10 times larger in the Mediterranean Sea than in the
26 middle of the ocean. In our regional configuration, SSH increments are purely statistical and
27 derived by the covariances between SSH (the prognostic variable of the model), temperature
28 and salinity implied by the ensemble of anomalies.

29

30 **2.5 Observational datasets**

31

1 The assimilated observations in MEDRYS consist of Sea Surface Temperature (SST)
2 maps, along track Sea Level Anomaly (SLA) data and in situ temperature and salinity
3 profiles. For each cycle, we assimilate the associated centered SST map coming from the
4 daily NOAA Reynolds 0.25° AVHRR-AMSR product (Reynolds et al., 2007). We assimilate
5 SST only each 1 degree to avoid correlation problem between observations. Moreover, we
6 noted a negative average bias of 0.2°C between AVHRR-AMSR product and the ERA-Interim
7 reanalysis SST that has been used for fluxes computation. For the sake of consistency
8 between fluxes and assimilated SST in MEDRYS, we decided to add 0.2°C to the AVHRR-
9 AMSR maps as a constant offset.

10

11 Along-track SLA delayed-time products, specifically reprocessed for Mediterranean Sea, and
12 distributed by AVISO (<http://www.aviso.altimetry.fr>) in April 2014 in the framework of
13 MyOcean project, are assimilated in MEDRYS. These products include along-track filtering
14 (low pass filtered with a cut-off wavelength of 65km for the whole domain) and along-track
15 sub-sampling (only one point over two is retained to avoid taking into account redundant
16 information). For these products, the reference period of the SLA is based on a 20-year [1993-
17 2012] period. Names and acronyms used in this paper as well as the measurement period of
18 each satellite are summarized in Table 3. The assimilation of SLA observation requires the
19 knowledge the observation error and of a Mean Dynamic Topography (MDT). As the
20 simulated Mediterranean Sea has a constant volume in the NM12 configuration, a volume
21 correction term is also needed for the computation of the observation operator in MEDRYS.
22 Concerning the observation error, we choose to not trust observations near the coastal areas.
23 The observation error is then artificially increased within 50km of the whole Mediterranean
24 coast. The mean surface reference used is a hybrid product between the CNES-CLS09 MDT
25 (Rio et al., 2011) adjusted with the data from the Gravity field and steady-state Ocean
26 Circulation Explorer (GOCE) and from the Mercator-Ocean 1/4° Reanalysis
27 GLORYS2V1 (Lellouche et al., 2013) representing the 1993-2012 period. In MEDRYS, the
28 volume correction consists in adding a term in the SLA observation operator, representing the
29 effect of the Glacial Isostatic Adjustment (GIA) and the barystatic effect due to the mass
30 intake of continental ice melting. The spatial fluctuations of the GIA are applied on the MDT
31 to compensate for the local deformation of the geoid due to the ongoing deformation of the
32 solid Earth (Peltier et al., 2008). For the global ocean on average, the correction is about -

1 0.3mm/year. In addition we also apply a correction to compensate the mass intake of
2 continental ice melting in the Mediterranean basin. On average, the mass intake corresponds
3 to a rise of 0.85 mm/year.

4
5 In situ temperature and salinity profiles come from the CORA4 (Cabanes et al., 2013) in situ
6 database provided by CORIOLIS data center from the start of the reanalysis up to December
7 2012. For the last 6 months we used the real-time database. A check through objective quality
8 control and a data thinning have been done on the dataset in CORA4. Indeed, for each
9 instrument, only one profile per day and within a 0.1° distance is selected. The best profile is
10 identified thanks to a set of objective criteria on measurement resolution and number of
11 measurements flagged as good along the profile. In addition to the quality check done by
12 CORIOLIS, SAM2 carries out a supplementary quality control on in situ observations. In
13 order to minimize the risk of erroneous data being assimilated, the system automatically
14 removes, through different criteria, the data too far from a seasonal climatology (Lellouche et
15 al., 2013). On average over the whole period, 79 observations of temperature per year and 16
16 observations of salinity per year are rejected by this supplementary quality control performed
17 by SAM2.

18
19 As for SLA, we choose to not assimilate surface salinity observations near coastal areas. Due
20 to how we model the continental freshwater intake along the coast (section 2.1), we apply a
21 coastal surface mask within which the salinity observations are artificially replace by the
22 hindcast value. This concept of pseudo observation near the coast has already been used in
23 Lellouche et al. (2013) to overcome the deficiencies of the background error, in particular for
24 poorly observed variables.

25 26 **3. Validation methodology and scientific assessment**

27 28 **3.1 Validation methodology**

1 During the MyOcean project, scientists have defined validation metrics by region and type
2 of product, including observational products. Many efforts were made to synthesize and
3 homogenise quality information in order to provide quality summaries and accuracy numbers.
4 All these rely on the same basis of metrics that can be divided into four main categories
5 derived from Crosnier and Le Provost (2007).

6
7 The consistency between two-system solutions or between a system and observations can be
8 checked by “eyeball” verification. This consists in comparing subjectively two instantaneous
9 or time mean spatial maps of a given parameter. Coherent spatial structures or oceanic
10 processes such as main currents, fronts and eddies are evaluated. This process is referred to as
11 CLASS1 metrics. The consistency over time is checked using CLASS2 metrics which include
12 comparisons of moorings time series, and statistics between time series. Space and/or time
13 integrated values such as volume and heat transports, heat content and eddy kinetic energy are
14 referred to as CLASS3. Their values are generally compared with literature values or values
15 obtained with past time observations such as climatologies or reanalyses. Finally, CLASS4
16 metrics give a measure of the real time accuracy of systems, by calculating various statistics
17 of the differences between all available oceanic observations (in situ or satellite datasets
18 before data thinning and online quality check) and their model equivalent at the time and
19 location of the observation. The validation procedure thus involves all classes of metrics. It
20 checks improvements between versions of a system, and ensures that a version is robust and
21 its performance stable over time.

22
23 Firstly, we present assimilation statistics directly coming from SAM2 and then results from
24 both NM12-FREE and MEDRYS (daily outputs for all variables and additional hourly
25 outputs for sea surface variables) are presented. As CLASS1 diagnostic, we thus focus on the
26 impact of the assimilation of SLA data on surface circulation. As CLASS3, the assessment of
27 the interannual variability is made using integrated heat and salt contents. Then a CLASS4
28 diagnostic is made using the entire CORA4 database (without data thinning/quality check)
29 and the high frequency surface variability is presented through a comparison to a fixed
30 mooring in the Gulf of Lions (CLASS2). Even if the assimilation process corrects a part of
31 the distance between the model and the observation, the fluxes play a major role in
32 determining the water masses in the Mediterranean Sea and are thereby a good indicator

1 regarding the quality of an experiment. That is why, as CLASS3, we point out in the last
2 section, the benefit of the assimilation in terms of transport through the Strait of Gibraltar.

3 4 5 **3.2 Scientific assessment**

6 7 **3.2.1 Assimilation Statistics**

8
9 We present here assimilation diagnostics to highlight that the reanalysis system is
10 stable and well constrained by the assimilated observations. In this section, the evolution of
11 the mean and the RMS innovation for all SLA, SST and in situ profiles are shown.

12
13 The mean and the RMS of SLA innovation are presented in Figure 3. The mean SLA
14 innovation has a slight linear decrease of 0.65mm/year. This suggests that the volume
15 correction (effect of the GIA and ice melting, see section 2.5) we applied is not accurate
16 enough. On average over the whole period, the mean SLA innovation shows then a slight
17 negative anomaly of -8mm. We also note a seasonal cycle. This is probably due to
18 inconsistency between ORAS4 interannual SSH fields in the Atlantic part and the assimilated
19 data but a part of this problem could also come from runoff forcing. If the seasonal variations
20 represented in the runoff climatological values are not realistic enough, the error in the intake
21 of water mass through the Mediterranean basin is directly transferred to the SLA innovation.
22 The RMS of the innovation is steady all along the reanalysis and close to 6.5cm. This result is
23 quite good, knowing that the standard deviation of observations over time is 8cm (not shown
24 here).

25
26 The main constraint on the SST consists in the assimilation of in situ surface data and gridded
27 maps derived from satellite measurements. Thus, for each cycle, we assimilate at least 243
28 values uniformly distributed every spatial degree and a variable amount of in situ surface data
29 from CORA (Figure 4). Before 2004, we note that the main part of assimilated data comes
30 from the satellite data. The mean satellite SST innovation is close to 0°C during the whole

1 period of the reanalysis. The RMS of innovation is about 0.7°C all along the time period and
2 exhibits a seasonal signal with 0.25°C amplitude whose maximum is reached at the end of
3 summer. The same diagnostic using in situ profile observation at the surface exhibits some
4 similar features but we note a weak positive bias between in situ and satellite data of about
5 0.12°C at the end of the period (the RMS and the mean values from in situ measurements are
6 only significant between 2005 and 2012).

7

8 Finally, we present data assimilation diagnostics for temperature and salinity profiles function
9 of the depth (Fig. 5 and 6). Diagnostics on the amount of assimilated data show that before
10 the Argo era, i.e. before about 2005, there are few profiles deployed in the Mediterranean Sea,
11 and most of them only reach 1000m depth. This being so, the mean innovation is close to zero
12 in average between the surface and 2000m depth for temperature and salinity. From 2005 to
13 the end of the experiment, we note a positive anomaly (of observation minus model) of about
14 0.2°C and 0.03 psu around 400m depth. According to Figure 5 and 6, this seems to result
15 from a propagation of anomalies from surface layers started in 2003. Those positive
16 anomalies at intermediate depths suggest that the Levantine Intermediate Water (LIW) in the
17 model is too cold and too fresh compared to assimilated data in this layer. Conversely, the
18 innovation in surface and deep layers shows a slight negative anomaly. On average, the RMS
19 of the innovation shows reasonable values compared to the mean innovation and the specified
20 observation errors but we note a clear seasonal variation, especially for temperature profiles.
21 During summer, the surface layers become more stratified. Due to the strong gradients, a
22 small variation in the trajectory of the ocean model is then more likely to drift from
23 observations and the RMS naturally increases. Moreover, the cold bias in surface associated
24 to a warm bias in subsurface illustrates that there is a lack of stratification in MEDRYS during
25 summer.

26

27 **3.2.2 Mean Sea Surface Height and surface circulation**

28

29 The mean Eddy Kinetic Energy (EKE) and the mean currents of MEDRYS and
30 NM12-FREE over the 1993-2012 period are shown in Fig. 7. A quick comparison between
31 NM12-FREE and MEDRYS mean EKE reveals that the assimilation process has a strong

1 impact in the western Mediterranean sub-basin. In NM12-FREE, a strong positive mean EKE
2 anomaly has been located North of Majorca Island. It corresponds to the fingerprint of a too
3 permanent anticyclonic eddy. Thanks to altimetric data, Pascual et al. (2002) identified such
4 an intense eddy in 1998 in the Balearic sub-basin but described it as a temporary event.
5 Actually, in 1998, this anticyclonic eddy develops in September due to circumstantial
6 atmospheric and oceanic conditions and disappears during cold seasons. The quasi-permanent
7 occurrence of this eddy in NM12-FREE experiment suggests that the model and its high
8 resolution atmospheric forcing ALDERA are able to produce it but not to dissipate it
9 afterward. This results in a large perturbation in the general circulation in western
10 Mediterranean in NM12-FREE. According to figure 7, the Liguro-Provençal current in
11 NM12-FREE is deflected at the southern limit of the Gulf of Lions and a significant part of
12 the Atlantic waters is driven along the Spanish coast. This influences the circulation in the
13 Algero-Provençal and the Alboran sub-basins. In MEDRYS, the assimilation process restores
14 realistic surface circulation. The Atlantic Water (AW) migrates into the western
15 Mediterranean trough the Strait of Gibraltar and reaches the Sicily channel through the
16 Algerian current remaining close to the African coast.

17

18 In the reanalysis, the mean EKE especially increases in the Ionian sub-basin compared to the
19 hindcast. This is partially due to the characteristic of the observation error we used in the
20 assimilation process (section 2.5). Around the center of the Ionian sub-basin the observation
21 error is not increased, compared to coastal areas. More energy and features are thus injected
22 by the assimilation process. We also notice that the Levantine sub-basin, and more
23 specifically both the Ierapetra and Pelops anticyclonic eddies, are more energetic suggesting
24 that the mesoscale circulation component have been increased thanks to the assimilation of
25 observational data.

26

27 **3.2.3 Integrated temperature and salinity**

28

29 Integrated temperature and salinity from two hydrographic products are compared
30 with MEDRYS and NM12-FREE. The two products are EN3 (Ingleby and Huddleston, 2007)
31 and IMEDEA (Jordà et al. 2016, submitted paper; the reconstruction methodology has been

1 described in Llasses et al., 2015). Both products differ in the details of the mapping algorithm
2 and the quality control applied to the observations. The difference between them can be
3 viewed as a first estimate of the uncertainties linked to the observational products, which
4 cannot be neglected (Jordà and Gomis, 2013; Llasses et al., 2015). Basin integrals of the
5 various products are compared whatever real data is present or not. Monthly evolution over
6 three different layers representing surface (0-150m), intermediate (150-600m) and deep
7 (600m-bottom) waters are shown in Fig. 8 and 9.

8

9 The time series of the averaged temperature between the surface and 150m depth in Fig. 8
10 point out the good representation of the seasonal cycle in both NM12-FREE and MEDRYS.
11 The phase and the magnitude of the seasonal cycle are consistent with the EN3 and IMEDEA
12 gridded products. In terms of mean value, the two experiments are very close and present a
13 positive bias compared to the gridded products. Indeed, in the 0-150m layer, the difference
14 between the simulations and EN3 is about 0.15°C and twice more compared to IMEDEA.
15 This is also consistent with the assimilation statistics of in situ profiles shown in section 3.2.1.
16 In the upper layer, the averaged salinity in MEDRYS and NM12-FREE is comparable with
17 that in EN3 and IMEDEA. However, between 1992 and 2013, MEDRYS show a slight
18 positive bias of about 0.02 psu whereas NM12-FREE show a slight negative bias of -0.03 psu
19 compared to the reference products. Before 1993, the hindcast presents a clear negative bias
20 of -0.07 psu. In 1993, the data assimilation corrects this surface salinity bias. The interannual
21 variability of the atmospheric water fluxes (Evaporation-Precipitation-Runoffs, not shown)
22 present a less evaporative period followed by a stronger one in the late 90's and early 2000's.
23 This leads to similar variability in the surface salt content in both MEDRYS and NM12-
24 FREE. As there are few in situ data, especially for salinity, the stronger evaporation combined
25 to a weak salinity constraint during the early 2000's leads to high surface salinization in
26 MEDRYS.

27

28 Concerning the intermediate waters, one clearly sees on Fig. 8 and 9, the drift in NM12-
29 FREE. The model in a free configuration tends to warm and salinize intermediate waters. The
30 assimilation of data restores good average values and realistic variability. It is interesting to
31 notice that despite poor data coverage in the early 90's, the assimilation system is able to
32 restore a realistic averaged salinity. As we noted in the section 3.2.1, we note a spurious

1 positive anomaly in the MEDRYS salinity in the early 2000's. Those too salty and too dense
2 waters have been formed in the surface layers and have been advected toward the bottom
3 layers. This bias is probably explained by a bad adjustment of the volume correction term of
4 the SLA model equivalent (section 2.5). In section 3.2.1, we noted that the mean SLA
5 innovation (obs-model) was decreasing, meaning that the simulated sea level trends to rise too
6 quickly compared to the observations. In response thereto, the system tends to compensate by
7 densifying surface waters. As the assimilation system is more constrained on temperature
8 (due to better data coverage) it has a strong effect on salinity. The resulting bias is also
9 detected in the bottom layer until 2005. Considering the small number of assimilated data
10 below 600m depth, the model is only slightly constrained beyond this depth, especially before
11 2005. Thus, the reanalysis is quite close to the hindcast in terms of tendency and mean value
12 for both temperature and salinity.

13

14 According to Fig. 8, it is difficult to establish whether, both the hindcast and the reanalysis,
15 are able to represent a realistic temperature in the deepest layer. Actually, we cannot clearly
16 distinguish any reference values as the two gridded products show different signals. However,
17 the two experiments present a linear trend of warming of about $4 \cdot 10^{-3} \text{ }^\circ\text{C/year}$ comparable to
18 EN3 for the 1993-2012 period IMEDEA presents a lower warming of about $1.5 \cdot 10^{-3} \text{ }^\circ\text{C/year}$.
19 In the deepest layer, EN3 and IMEDEA show similar mean salinity (respectively 38.63 psu
20 and 38.64 psu between 1979 and 2010) and a similar interannual variability. NM12-FREE
21 presents a linear salinization over the whole period of the experiment in agreement with the
22 gridded product ($1.2 \cdot 10^{-3} \text{ psu/year}$). With a limited number of data to assimilate, MEDRYS
23 show an episode of high salinization from 1997 to 2004. Thanks to better data coverage after
24 2005, the reanalysis becomes more constrained and show a more realistic average salinity, in
25 accordance to our reference products.

26

27 Following Adani et al. 2011, the vertical distribution of the temperature and salinity
28 anomalies is then presented in Fig. 10 and 11. Temperature and salinity anomalies have been
29 computed with respect to the monthly cycle of the MEDATLAS-1979 climatology, from
30 which the October month has been taken to initialise NM12-FREE (see section 2.2). These
31 figures complete the vertical view given by Fig. 5 and 6 which were computed only at
32 observation locations, and the integrated view given by Fig. 8 and 9. Moreover, this kind of

1 diagnostics is presented in Adani et al. (2011) allowing thus a qualitative comparison of two
2 available reanalyses. For temperature, both NM12-FREE and MEDRYS show a similar
3 behaviour in the surface layer (above 100m depth); we can thus attribute these anomalies to
4 the model configuration (for instance issues with the vertical mixing) and to interannual
5 variations, both simulations being forced by the same realistic atmospheric forcings in
6 surface. In the intermediate layer, NM12-FREE becomes slowly warmer and warmer, starting
7 with a cold anomaly of about -0.1°C in 1993 and ending with a warm anomaly of about
8 $+0.2^{\circ}\text{C}$ in 2013, in the core of the LIW layer. For MEDRYS, this core is too cold of about
9 0.2°C to -0.1°C , this anomaly becoming smaller at the end of the period. In the bottom layer,
10 NM12-FREE remains slightly colder than its initial state, around -0.1°C , whereas MEDRYS
11 shows a slight warming during the 20 years, in agreement with Fig.8.

12

13 For salinity, again the anomalies above 100m depth are similar in both simulations; the
14 succession of positive and negative anomalies can be related to interannual variability.
15 Nevertheless, the surface layer is more salty in MEDRYS than in NM12-FREE, especially
16 during the last years. In the intermediate layer, around the core of the LIW layer, NM12-
17 FREE becomes saltier and saltier during the 20 years, from $+0.05$ psu in 1993 up to $+0.15$ psu
18 at the end of the period. In MEDRYS the intermediate anomalies are negative, around -0.05
19 psu, and located deeper than in NM12-FREE, around 650m depth, thus at the base of the LIW
20 layer. In the bottom layer (below 1200m), NM12-FREE has small salinity anomalies around 0
21 psu, become slightly negative below 2000m between 2003 and 2007, and slightly positive
22 between 1200m and 2000m at the end of the period, displaying interannual variability. In
23 MEDRYS, the deep layer is slightly saltier, with a small trend during the period, starting with
24 anomalies around 0 psu in 1993 and ending with anomalies up to $+0.1$ psu. Moreover, the
25 positive anomalies in the surface layer in MEDRYS around year 2000 seems to propagate
26 downwards (as seen in Fig.9), leading to the end of the negative anomaly in the intermediate
27 layer between 2001 and 2005 and to a stronger positive anomaly in the bottom layer between
28 2002 and 2006.

29

30 We can qualitatively compare Fig.10 and 11 to a similar diagnostic performed by Adani et al.
31 (2011) (their figures 8 and 9); the common period is 1993-2007. One can notice similar
32 patterns in both reanalyses: high variability in surface layer, a slightly too cold intermediate

1 layer, and a deep layer becoming warmer and saltier during the simulated period, the
2 amplitude of the anomalies being smaller in MEDRYS. As these reanalyses are performed
3 with different numerical modelling choices, different atmospheric forcing and different
4 assimilation schemes, these common features could be related to realistic physical processes,
5 which could be interesting to assess in a common dedicated work.

8 **3.2.4 Temperature and salinity vertical profiles**

10 The model equivalent at the time and spatial location of the observations has been
11 computed from daily averaged outputs. Mean and RMS differences over the whole
12 Mediterranean basin were computed for 3 layers (0-150m, 150-600m, 600-4000m) for
13 temperature and salinity profiles (CLASS4) and are presented in Figures 12 and 13. In order
14 to evaluate the improvement with respect to a constant state, we applied the same process
15 with the profiles from MEDATLAS-1998. The MEDATLAS-1998 temperature and salinity
16 fields are the initial states of short simulations used for process studies such as in Beuvier at
17 al. (2012a). Those fields have been obtained pondering by a low pass filtering with a time-
18 window of three years, the MEDATLAS data covering the 1997-1999 period. The choice of
19 centering the climatology on the late 90's corresponds to a compromise between a recent year
20 (before 2002, the last field in MEDATLAS) and a sufficient data coverage in both
21 temperature and salinity, knowing that the uncertainty associated with the MEDATLAS fields
22 increases after 2000. Only a daily dataset, checked through objective quality control, have
23 been assimilated in MEDRYS. Large differences may appear locally in the CLASS4 scores
24 with spurious observations. CLASS4 results complement here the statistics made against one
25 week forecasts in section 3.2.1.

27 We first assess the mean and RMS temperature differences between the analysis and the
28 observations in Figure 12. Concerning the layer-averaged mean differences, results are not
29 fully consistent with comparisons made with integrated content in section 3.2.3. Indeed, those
30 statistics show that, on average, MEDRYS is very close to the observations (at the location of
31 the observations). We only note a significant negative bias of 0.03°C in the layer 150/600m

1 on average over the period 1993-2012. The mean temperature difference in the two first layers
2 of the reanalysis reproduces the interannual variability present in the observations. As
3 MEDATLAS-1998 is a climatology, the magnitude of the oceanic interannual variability is
4 then represented by the blue curve. We also point out that, in average, no particular
5 temperature bias occurred in the deepest layer in MEDRYS. This highlights that the system is
6 well constrained and efficiently responds to the assimilation of in situ profiles. As in average
7 MEDRYS remains close to temperature measurements, that also confirms that the reference
8 products shown in the section 3.2.3 are subject to uncertainties, especially in the deepest
9 layers where the estimated mean temperature may vary widely from a product to another. In
10 term of mean salinity (Fig. 13), MEDRYS is also close to the observations in the deepest
11 layers but, as expected, presents a slight positive bias of about 0.02psu between the surface
12 and 150m depth. When we compared integrated salinity of the reanalysis with other gridded
13 products, we noted a spurious salinization in MEDRYS in the early 2000s that propagated
14 toward deeper layers. In average, the CLASS4 mean difference in salinity is only about
15 0.1psu between the surface and 150m depth and is not noticeable below. Assuming that the
16 major part of the salinity observations are used in both MEDRYS and the reference gridded
17 products, this suggests that the signal of the deeper salinization is not in the observations but
18 is a consequence of the propagation of the simulated surface anomaly through the ocean
19 model. However, as the uncertainties in the salinity products are large (Llasses et al., 2015),
20 it cannot be discarded that the observationnal products missed that change.

21
22 The RMS of the difference is quite good both in temperature and salinity considering the
23 variability in the different layers. However, we note that the RMS of the difference in salinity
24 increases in the waters deeper than 600m, meaning that, despite a realistic estimation of the
25 mean value, the spatial variability is not robust. This can be explained by the lack of salinity
26 measurements and the poor data coverage in Mediterranean Sea under 1000m depth,
27 especially before 2005. In average, MEDRYS presents a lower RMS of the difference of
28 temperature and salinity than MEDATLAS-1998. It is not surprising considering that
29 MEDATLAS-1998 is composed of climatological monthly fields and does not represent the
30 variability of the Mediterranean Sea along the whole period of 21 years. In the first 150m, the
31 RMS of the difference in MEDRYS increases with the summertime stratification.

32

3.2.5 High frequency variability: comparison at LION buoy

We show here the ability of NM12-FREE and MEDRYS to reproduce the high frequency variability at the surface in the Mediterranean basin. In Figure 14, we compare the high frequency measurements of SST and SSS at the LION buoy (first level of CTD measurements) during HyMeX SOP2 (Special Observation Period 2 from 01/27/2013 to 03/15/2013) to the hourly outputs of the two numerical experiments at the same location. As we noted in paragraph 2.5, the real-time database have been assimilated in 2013. Data from LION buoy were not yet available in real-time and were not assimilated. Note, that this kind of punctual comparison don't allow to assess the high frequency variability over the whole domain of the simulations, but only give an overview of their own abilities.

For both SST and SSS comparisons, MEDRYS is slightly closer to the independent observations than the hindcast, in terms of mean values and variability. Indeed, the mean surface water of MEDRYS shows a positive bias of 0.07°C and 0.03psu while NM12-FREE shows negative biases which are larger in magnitude (0.13°C and 0.06psu). The major part of the mean bias in SSS between MEDRYS and the observations can be explained by the large difference during January ($+0.1\text{psu}$ in average) because the mean bias afterward is very weak (less than 0.01psu). Indeed, we notice a strong jump in the observed SSS the 30th of January ($+0.04\text{psu}$) corresponding to a salinity sensor repair (personal communication from M.N. Bouin). The water-pump was defective and affected the conductivity measurement. Assuming that a constant negative bias of $0,04\text{psu}$ contaminated the observation during January, MEDRYS finally presents very good results in SSS during SOP2 at the LION buoy.

Regarding the SST, MEDRYS has a better correlation with LION buoy than NM12-FREE (respectively 76% and 31%). However, MEDRYS and NM12-FREE show a similar correlation for SSS of 78%. For all that, the hindcast is very similar to MEDRYS in the second half of SOP2. This is not surprising since the variability at the surface is controlled by fluxes (identical for both experiments) during the mixed phase of the convection. We especially note the good representation in phase and amplitude of the diurnal variations of SST. This is especially obvious around the 20th February and during many days in March

1 during a temporary restratification period, when the diurnal cycle of ALDERA heat fluxes
2 have a higher daily amplitude (beginning of spring season).

3

4 **3.2.6 Transport through the Strait of Gibraltar**

5

6 We present here water, heat and salt transport through the Strait of Gibraltar at 5.5°W
7 in Figure 15. Heat and salt fluxes are computed from temperature (T) and salinity (S) using
8 equations 1 and 2. U_x represents the zonal component of the current at 5.5°W, ρ_0 is the
9 reference sea water density (1020 Kg.m⁻³), S_{med} and V_{med} are respectively the surface and the
10 volume of the simulated Mediterranean Sea and N_{sec} is the number of seconds in a year.
11 Characteristics of the inflow (surface layers) and the outflow (deep layers) and the difference
12 between the two (net flow) are presented. The interface between inflow and outflow has been
13 determined using the horizontal velocity through the strait at daily time-scale.

14

15 Eq. 1 :
$$HeatFlux_{gib} = \frac{\rho_0 C_p}{S_{med}} \iint T(y, z) U_x(y, z) dy dz$$

16

17 Eq. 2 :
$$SaltFlux_{gib} = \frac{N_{sec}}{V_{med}} \iint S(y, z) U_x(y, z) dy dz$$

18

19 Although the characteristics of the ocean are the same in the buffer zone in the two
20 experiments, the amplitude of both inflow and outflow has been improved thanks to data
21 assimilation in MEDRYS (Fig. 15). Despite the realistic value of the net flow through the
22 Strait of Gibraltar, outflow and inflow are underestimated in NM12-FREE in comparison with
23 recent results published (Soto-Navarro et al., 2010, 2014). According to those studies, the
24 acceptable range for inflow and outflow at Gibraltar Strait are respectively [+0.76 ; +0.86]Sv
25 and [-0.84 ; -0.72]Sv. The reason of having a more accurate exchange at Gibraltar in
26 MEDRYS is that the density difference between the inflowing and outflowing waters is larger
27 (-2.34 kg/m³ in MEDRYS and -2.30 kg/m³ in NM12-FREE). In terms of net heat transport,
28 the reanalysis and the hindcast (respectively 6.6±0.4 W/m² and 5.5±0.4 W/m²) are consistent
29 with MacDonald et al. (1994). We also compare the properties of the inflow in MEDRYS and

1 NM12-FREE with results from Soto-Navarro et al. (2014) at the sill of Espartel. They used,
2 inter alia, the experiment NM12-ARPERA. This simulation show similar results with an
3 interface around 150m depth. At this particular depth, we also report similar results with AW
4 at 15.4°C and 36.7psu in MEDRYS and at 15.5°C and 36,5psu in NM12-FREE.

5
6 The net salt transport through the Strait of Gibraltar at 5.5°W is $1.8 \pm 2.8 \cdot 10^{-3}$ psu/year in
7 MEDRYS and $3.0 \pm 2.6 \cdot 10^{-3}$ psu/year in NM12-FREE (Fig. 14). Assuming that the
8 Mediterranean volume is constant, the evolution of Mediterranean salinity is directly linked to
9 the net transport of salt through the Strait of Gibraltar. The trend in salinity (Δs_{ref}) of the
10 reference hydrographic gridded products (EN3 and IMEDEA) over the whole basin serves as
11 a way to estimate a reference net salt transport entering at Gibraltar ($SaltFlux_{gib}$ from Eq.2),
12 using $SaltFlux_{gib} = \Delta s_{ref}$. From the hydrographic products, we estimate a reference net salt
13 intake at approximately $1.7 \cdot 10^{-3}$ psu/year between 1993 and 2012. In MEDRYS, the averaged
14 net salt transport through the Strait of Gibraltar is very close to this reference value but this is
15 not representative of the evolution of the salinity over the whole basin because of the addition
16 of salinity increments coming from the assimilation scheme. Indeed, NM12-FREE and
17 MEDRYS have a similar trend in salinity in spite of a different net salt transport at Gibraltar.

18

19 **4. Discussion and conclusion**

20

21 This study describes the configuration and the quality of the high resolution reanalysis
22 MEDRYS and its companion hindcast NM12-FREE, for the Mediterranean Sea over the
23 period 1992-2013. Both simulations have a common configuration: a high-resolution oceanic
24 model NEMOMED12 relaxed in the Atlantic buffer zone to ORAS4 interannual fields and
25 forced at the surface with the homogeneous and high-resolution ALDERA atmospheric
26 fluxes. The 21 years of the reanalysis have been produced using in situ profiles from the
27 CORA4 database, SST maps from the daily NOAA AVHRR-AMSR product and along-track
28 SLA from SSALTO/DUACS associated to SAM2 the assimilation scheme from Mercator
29 Océan. The 12-km and 3-hour spatio-temporal resolution of ALDERA fields allows
30 MEDRYS to explicitly reproduce diurnal cycle, and thus SST, and to simulate the impact of
31 local winds on coastal oceanic areas. As we pay a special attention in reducing sources of

1 inhomogeneity in the atmospheric forcing ALDERA dataset along the whole 1979-2013, this
2 suggests to trust in the consistency of the interannual variability of processes known to be
3 driven by air-sea interactions (mixed layer variability, surface circulation variability, etc.) in
4 MEDRYS.

5

6 The validation process has highlighted the good results of the reanalysis in terms of mean
7 circulation and integrated heat and salt contents. The data assimilation has a positive impact,
8 especially in the western basin, where it restores a correct circulation of the Liguro-Provençal
9 current and of the Algerian current. The assimilation process leads to stronger mesoscale
10 variability in the Ionian and Levantine sub-basin, especially at the location of Ierapetra and
11 Pelops eddies. Looking at in situ profiles, the reanalysis shows a realistic water masses at
12 intermediate depths, unlike in the hindcast. In this layer, the simulation without assimilation
13 NM12-FREE drifts from the observations and show a strong positive trend in both
14 temperature and salinity. Transports through the Strait of Gibraltar have also been improved
15 in the reanalysis. Despite the same forcing in the Atlantic buffer zone, both inflow and
16 outflow in MEDRYS have been increased compared to NM12-FREE and are now comparable
17 to historical values. The net heat and salt budgets through the strait are also consistent with
18 independent products. The improvement of the Atlantic/Mediterranean fluxes at Gibraltar
19 ensures a better budget in the Mediterranean Sea.

20

21 We showed that surface waters in MEDRYS were in average too salty (about 0.02psu). This
22 problem probably comes from the adjustment of the volume correction during the
23 computation of SLA model equivalent. We also point out that it had inconsistencies between
24 ORAS4 interannual fields in the buffer zone and the assimilated data. To correct for those
25 inconsistencies, it will be necessary to apply a correction to the ORAS4 SSH fields in order to
26 better represent the seasonal variations of sea level in the Mediterranean. In further version of
27 MEDRYS, we simply propose to correct the seasonal cycle and the trends of sea level
28 anomalies in ORAS4 in order to match with altimetry observations in the buffer zone.
29 According to additional works (not shown in this study), we realized that SLA innovations
30 were strongly correlated with the mean wind patterns (Mistral-Tramontane, Aegean winds),
31 suggesting that the hydraulic constraint component is not negligible in the Mediterranean Sea.
32 Knowing that, the configuration of SAM2 should be adjusted in order to take into account the

1 wind component in SSH. Moreover, as the effect of the wind at high frequency has been
2 filtered from the SSALTO/DUACS database, it would be also necessary to filter it in the
3 model.

4

5 **Acknowledgements**

6

7 We acknowledge the two anonymous reviewers for their comments and suggestions which
8 helped to improve this article. This work is a contribution to the HyMeX program
9 (HYdrological cycle in The Mediterranean EXperiment) through INSU-MISTRALS support
10 and the Med-CORDEX program (COordinated Regional climate Downscaling EXperiment –
11 Mediterranean region). This research has received funding from the French National Research
12 Agency (ANR) project REMEMBER (contract ANR-12-SENV-001). All the ALDERA
13 outputs are openly available through the Med-CORDEX database (www.medcordex.eu).

1 **References**

- 2 Adani, M., Dobricic, S., Pinardi, N., 2011. Quality assessment of a 1985–2007 Mediterranean
3 Sea reanalysis. *Journal of Atmospheric and Oceanic Technology* 28 (4), 569–589.
4 <http://dx.doi.org/10.1175/2010JTECHO798.1>.
- 5 Auger P.A., Ulses C., Estournel C., Stemman L., Somot S., Diaz F. (2014) Interannual control
6 of plankton ecosystem in a deep convection area as inferred from a 30-year 3D modeling
7 study: winter mixing and prey/predator in the NW Mediterranean. *Progress in Oceanography*:
8 12-27, DOI: 10.1016/j.pocean.2014.04.004
- 9 Ayoub, N., Le Traon, P.-Y., De Mey, P., 1998. A description of the Mediterranean surface
10 variable circulation from combined ers-1 and topex/poseidon altimetric data. *Journal of*
11 *Marine Systems* 18 (1–3),3–40,
12 <http://www.sciencedirect.com/science/article/pii/S0924796398800043>"<http://www.sciencedirect.com/science/article/pii/S0924796398800043>.
- 14 Balmaseda, M. A., K. E. Trenberth, and E. Källén (2013), Distinctive climate signals in
15 reanalysis of global ocean heat content, *Geophys. Res. Lett.*, 40, 1754–1759,
16 doi:10.1002/grl.50382.
- 17 Barnier B., L. Siefridt, P. Marchesiello, 1995. Thermal forcing for a global ocean circulation
18 model using a three-year climatology of ECMWF analyses. *Journal of Marine Systems*,
19 Volume 6, Issue 4, June 1995, Pages 363–380.
- 20 Béranger, K., L. Mortier, and M. Crépon, 2005. Seasonal variability of water transport
21 through the Straits of Gibraltar, Sicily and Corsica, derived from a high-resolution model of
22 the Mediterranean circulation, *Progress in Oceanography*, 66, 341–364.
- 23 Béranger, K., Y. Drillet, M-N. Houssais, P. Testor, R. Bourdallé-Badie, B. Alhammoud, A.
24 Bozec, L. Mortier, P. Bouruet-Aubertot, and M. Crépon (2010), Impact of the spatial
25 distribution of the atmospheric forcing on water mass formation in the Mediterranean Sea,
26 *Journal of Geophysical Research*, 115(C12041). doi:10.1029/2009JC005648.
- 27 Beuvier, J., F. Sevault, M. Herrmann, H. Kontoyiannis, W. Ludwig, M. Rixen, E. Stanev, K.
28 Béranger, and S. Somot, 2010. Modeling the Mediterranean Sea interannual variability during
29 1961-2000 : Focus on the Eastern Mediterranean Transient, *Journal of Geophysical Research*,
30 115(C08017), doi :10.1029/2009JC005950.

1 Beuvier J., Béranger K., Lebeaupin-Brossier C., Somot S., Sevault F., Drillet Y., Bourdalle-
2 Badie R., Ferry N., Lyard F., 2012a. Spreading of the Western Mediterranean Deep Water
3 after winter 2005: time scales and deep cyclone transport. *J Geophys Res-Oceans*.
4 doi:10.1029/2011JC007679.

5 Beuvier, J., C. Lebeaupin-Brossier, K. Béranger, T. Arsouze, R. Bourdallé-Badie, C. Deltel,
6 Y. Drillet, P. Drobinski, N. Ferry, F. Lyard, F. Sevault, and S. Somot, 2012b. MED12,
7 oceanic component for the modeling of the regional Mediterranean Earth System, Mercator
8 Ocean Quaterly Newsletter, 46, Octobre 2012, 60-66.

9 Cabanes, C., Grouazel, A., von Schuckmann, K., Hamon, M., Turpin, V., Coatanoan, C.,
10 Paris, F., Guinehut, S., Boone, C., Ferry, N., de Boyer Montégut, C., Carval, T., Reverdin, G.,
11 Pouliquen, S., and Le Traon, P.-Y., 2013. The CORA dataset: validation and diagnostics of
12 in-situ ocean temperature and salinity measurements, *Ocean Sci.*, 9, 1-18, doi:10.5194/os-9-1-
13 2013.

14 Casella E., A. Molcard, A. Provenzale (2011) Mesoscale vortices in the Ligurian Sea and
15 their effect on coastal upwelling processes, *Journal of Marine Systems*, 88, 12–19,
16 doi:10.1016/j.jmarsys.2011.02.019.

17 Ciappa A. C. (2009) Surface circulation patterns in the Sicily Channel and Ionian Sea as
18 revealed by MODIS chlorophyll images from 2003 to 2007 , *Continental Shelf Research* 29,
19 2099–2109 , doi:10.1016/j.csr.2009.08.002 .

20 Colin, J., M. Déqué, R. Radu and S. Somot, 2010. Sensitivity study of heavy precipitation in
21 Limited Area Model climate simulations: influence of the size of the domain and the use of
22 the spectral nudging technique. *Tellus A*, 62: 591–604. doi: 10.1111/j.1600-
23 0870.2010.00467.x.

24 Crosnier, L. and Le Provost, C., 2007. Inter-comparing five forecast operational systems in
25 the North Atlantic and Mediterranean basins: the MERSEA-strand1 methodology, *J. Mar.*
26 *Syst.*, 65, 354–375.

27 Dee, D. P., S. M. Uppala, A. J. Simmons, P. Berrisford, P. Poli, S. Kobayashi, U. Andrae, M.
28 A. Balmaseda, G. Balsamo, P. Bauer, P. Bechtold, A. C. M. Beljaars, L. van de Berg, J.
29 Bidlot, N. Bormann, C. Delsol, R. Dragani, M. Fuentes, A. J. Geer, L. Haimberger, S. B.
30 Healy, H. Hersbach, E. V. Hólm, L. Isaksen, P. Kållberg, M. Köhler, M. Matricardi, A. P.
31 McNally, B. M. Monge-Sanz, J.-J. Morcrette, B.-K. Park, C. Peubey, P. de Rosnay, C.

1 Tavolato, J.-N. Thépaut, F. Vitart, 2011. The ERA-Interim reanalysis: configuration and
2 performance of the data assimilation system. *Q.J.R. Meteorol. Soc.*, 137: 553–597. doi:
3 10.1002/qj.828.

4 Drobinski P. Ducrocq V., Alpert P., Anagnostou E., Béranger K., Borga M., Braud I., Chanzy
5 A., Davolio S., Delrieu G., Estournel C., Filali Boubrahmi N., Font J., Grubisic V., Gualdi S.,
6 Homar V., Ivancan-Picek B., Kottmeier C., Kotroni V., Lagouvardos K., Lionello P., Liasat
7 M.C., Ludwig W., Lutoff C., Mariotti A., Richard E., Romero R., Rotunno R., Roussot O.,
8 Ruin I., Somot S., Taupier-Letage I., Tintoré J., Uijlenhoet R., Wernli H. (2013) HyMeX, a
9 10-year multidisciplinary program on the Mediterranean water cycle, *Bulletin of the*
10 *American Meteorological Society*, doi: <http://dx.doi.org/10.1175/BAMS-D-12-00242.1>.

11 Dufau-Julliand C., P. Marsaleix, A. Petrenko, I. Dekeyser (2004) Three-dimensional
12 modeling of the Gulf of Lion’s hydrodynamics (northwest Mediterranean) during January
13 1999 (MOOGLI3 Experiment) and late winter 1999: Western Mediterranean Intermediate
14 Water’s (WIW’s) formation and its cascading over the shelf break , *JOURNAL OF*
15 *GEOPHYSICAL RESEARCH*, VOL. 109, C11002, doi:10.1029/2003JC002019, 2004

16 Durrieu de Madron, X., et al., 2013. Interaction of dense shelf water cascading and open-sea
17 convection in the northwestern Mediterranean during winter 2012. *Geophys. Res. Lett.*, 40,
18 1379–1385, doi:10.1002/grl.50331.

19 Elguindi N., Somot S., Déqué M., Ludwig W. (2011) “Climate change evolution of the
20 hydrological balance of the Mediterranean, Black and Caspian Seas: impact of climate model
21 resolution” *Clim. Dyn.*, 36 (1-2), 205-228, doi: 10.1007/s00382-009-0715-4

22 Estournel C., X. Durrieu de Madron, P. Marsaleix, F. Auclair, C. Julliand, and R. Vehil
23 (2003) Observation and modeling of the winter coastal oceanic circulation in the Gulf of Lion
24 under wind conditions influenced by the continental orography (FETCH experiment)
25 *JOURNAL OF GEOPHYSICAL RESEARCH*, VOL. 108, NO. C3, 8059,
26 doi:10.1029/2001JC000825, 2003.

27 Estournel C. , F. Auclair , M. Lux , C. Nguyen , and P. Marsaleix (2009) “Scale oriented”
28 embedded modeling of the North-Western Mediterranean in the frame of MFSTEP , *Ocean*
29 *Sci.*, 5, 73–90, 2009, www.ocean-sci.net/5/73/2009/.

1 Fernandez V. D. E. Dietrich, R. L. Haney, J. Tintore (2005) Mesoscale, seasonal and
2 interannual variability in the Mediterranean Sea using a numerical ocean model , Progress in
3 Oceanography, doi:10.1016/j.pocean.2004.07.010.

4 Giorgi, F., 2006. Climate change hot-spots, Geophys. Res. Lett., 33, L08707, doi:
5 <http://dx.doi.org/10.1029/2006GL025734>"10.1029/2006GL025734.

6 Hamad, N, Millot, C , Taupier-Letage, I (2005) A new hypothesis about the surface
7 circulation in the eastern basin of the Mediterranean Sea, Progress in Oceanography, 66, 287-
8 298.

9 Harzallah, A., Alioua, M., & Li, L. (2014). Mass exchange at the Strait of Gibraltar in
10 response to tidal and lower frequency forcing as simulated by a Mediterranean Sea model.
11 Tellus A, 66.

12 Herrmann, M. J., and S. Somot, 2008. Relevance of ERA40 dynamical downscaling for
13 modeling deep convection in the Mediterranean Sea, Geophysical Research Letters,
14 35(L04607), doi:10.1029/2007GL03244.

15 Herrmann, M., F. Sevault, J. Beuvier, and S. Somot, 2010. What induced the exceptional
16 2005 convection event in the northwestern Mediterranean basin ? Answers from a modeling
17 study. Journal of Geophysical Research, 115(C12051), doi :10.1029/2010JC006162.

18 Herrmann, M., S. Somot, S. Calmanti, C. Dubois, and F. Sevault, 2011. Representation of
19 spatial and temporal variability of daily wind speed and of intense wind events over the
20 Mediterranean Sea using dynamical downscaling : impact of the regional climate model
21 configuration, Natural Hazards and Earth System Sciences, 11, 1983–2001, doi:
22 10.5194/nhess- 11-1983-2011.

23 Ingleby, B. and M. Huddleston, 2007. Quality control of ocean temperature and salinity
24 profiles - historical and real-time data. Journal of Marine Systems, 65, 158–175.
25 doi:10.1016/j.jmarsys.2005.11.019.

26 Jordà G. and D. Gomis, 2013. On the interpretation of the steric and mass components of sea
27 level variability: The case of the Mediterranean basin. Journal of Geophysical Research, Vol.
28 118, Issue 2, 953-963. 10.1002/jgrc.20060

1 Josey, S. A., S. Somot, and M. Tsimplis, 2011. Impacts of atmospheric modes of variability
2 on Mediterranean Sea surface heat exchange, *Journal of Geophysical Research*, 116(C02032),
3 doi:10.1029/2010JC006685.

4 Langlais, C., B. Barnier, J.M. Molines, P. Fraunié, D. Jacob, S. Kotlarski, 2009. Evaluation of
5 a dynamically downscaled atmospheric reanalyse in the prospect of forcing long term
6 simulations of the ocean circulation in the Gulf of Lions, *Ocean Modelling*, Volume 30, Issue
7 4, Pages 270-286, ISSN 1463-5003. <http://dx.doi.org/10.1016/j.ocemod.2009.07.004>.

8 Llasses, J, G. Jordà, D. Gomis 2015. Skills of different hydrographic networks in capturing
9 changes in the Mediterranean Sea at climate scales. *Climate Research*. Vol. 63: 1–18, 2015
10 doi: 10.3354/cr01270Lebeaupin Brossier, C., K. Béranger, C. Deltel, and P. Drobinski, 2011.
11 The Mediterranean response to different space-time resolution atmospheric forcings using
12 perpetual mode sensitivity simulations, *Ocean Modelling*, 36, 1–25,
13 doi :10.1016/j.ocemod.2010.10.008.

14 Lebeaupin Brossier, C., K. Béranger and P. Drobinski, 2012. Sensitivity of the northwestern
15 Mediterranean Sea coastal and thermohaline circulations simulated by the 1/12° -resolution
16 ocean model NEMO-MED12 to the spatial and temporal resolution of atmospheric forcing,
17 *Ocean Modelling*, 43-44, 94–107, doi :10.1016/j.ocemod.2011.12.007.

18 Lebeaupin Brossier C., Arsouze T, Béranger K, Bouin M-N., Bresson E., Ducrocq V.,
19 Giordani H., Nureta M., Rainaud R., Taupier-Letage I. (2014) Ocean mixed layer responses to
20 intense meteorological events during HyMeX-SOP1 from a high-resolution ocean simulation,
21 *Ocean Modelling*, Vol 84, 84-103.

22 Lellouche J.M., O. Le Galloudec, M. Drévillon, C. Régnier, E. Greiner, G. Garric, N. Ferry,
23 C. Desportes, C.-E. Testut, C. Bricaud, R. Bourdallé-Badie, B. Tranchant, M. Benkiran, Y.
24 Drillet, A. Daudin and C. De Nicola, 2013. Evaluation of global monitoring and forecasting
25 systems at Mercator Océan. *Ocean Sci.*, 9, 57–81. doi:10.5194/os-9-57-2013.

26 L'Hévéder, B., L. Li, F. Sevault and S. Somot, 2013. Interannual variability of deep
27 convection in the Northwestern Mediterranean simulated with a coupled AORCM. *Clim.*
28 *Dyn.*, Vol. 41, Issue 3-4, pp937-960.

29 Louis, J.-F. 1979. A parametric model of vertical eddy fluxes in the atmosphere. *Boundary*
30 *Layer Meteorol.* 17, 187202.

- 1 Ludwig, W., E. Dumont, M. Meybeck, and S. Heussner, 2009. River discharges of water and
2 nutrients to the Mediterranean and Black Sea : Major drivers for ecosystem changes during
3 past and future decades ?, *Progress in Oceanography*, 80, 199–217.
- 4 Lyard, F., F. Lefevre, T. Letellier, and O. Francis, 2006. Modelling the global ocean tides :
5 modern insights from FES2004, *Ocean Dynamics*, 56(5-6), doi :10.1007/s10236-006-0086-x.
- 6 Macdonald, A. M., J. Candela, and H. L. Bryden 1994. An estimate of the net heat transport
7 through the Strait of Gibraltar, in *Seasonal and Interannual Variability of the Western*
8 *Mediterranean Sea Coastal and Estuarine Studies*, Coastal Estuarine Stud., vol. 46, edited by
9 P. E. La Violette et al., pp. 13–32, AGU, Washington, D. C.
- 10 Madec, G., Delecluse, P., Imbard, M., Levy, C., 1997. OPA, release 8, Ocean general
11 circulation reference manual. Technical Report 96/xx, LODYC/IPSL, France.
- 12 Madec , G. and The-NEMO-Team (2008) NEMO, Technical report (IPSL), France.
- 13 Mariotti, A., N. Zeng, J. Yoon, V. Artale, A. Navarra, P. Alpert and L. Li, 2008.
14 Mediterranean water cycle changes: transition to drier 21st century conditions in observations
15 and CMIP3 simulations. *Res. Lett.* 3 044001 doi:10.1088/1748-9326/3/4/044001.
- 16 Marullo, S., E. Napolitano, R. Santoleri, B. Manca, and R. Evans, 2003. Variability of Rhodes
17 and Ierapetra Gyres during Levantine Intermediate Water Experiment: Observations and
18 model results, *J. Geophys. Res.*, 108, 8119, doi:10.1029/2002JC001393, C9.
- 19 Millot C. and Taupier-Letage (2005) *Circulation in the Mediterranean Sea*, The handbook of
20 environmental chemistry, Vol.1, 29-66, Springer-Verlag.
- 21 Nabat, P., S. Somot, M. Mallet, A. Sanchez-Lorenzo, and M. Wild, 2014. Contribution of
22 anthropogenic sulfate aerosols to the changing Euro-Mediterranean climate since 1980,
23 *Geophys. Res. Lett.*, 41, 5605–5611, doi:10.1002/2014GL060798.
- 24 Ourmières Y, Zakardjian B, Béranger K, Langlais C (2011) Assessment of a NEMO-based
25 downscaling experiment for the North-Western Mediterranean region: impacts on the
26 Northern Current and comparison with ADCP data and altimetry products. *Ocean Modelling*
27 39, 386-404.
- 28 Palmiéri, J., Orr, J. C., Dutay, J.-C., Béranger, K., Schneider, A., Beuvier, J., and Somot, S.,
29 2015. Simulated anthropogenic CO2 storage and acidification of the Mediterranean Sea,
30 *Biogeosciences*, 12, 781-802, doi:10.5194/bg-12-781-2015.

1 Papadopoulos Vassilis P., Simon A. Josey, Aristides Bartzokas, Samuel Somot, Simon Ruiz,
2 and Paraskevi Drakopoulou, 2012. Large-Scale Atmospheric Circulation Favoring Deep- and
3 Intermediate-Water Formation in the Mediterranean Sea. *J. Climate*, 25, 6079–6091. doi:
4 <http://dx.doi.org/10.1175/JCLI-D-11-00657.1>.

5 Pascual, A., B. Buongiorno Nardelli, G. Larnicol, M. Emelianov, and D. Gomis, 2002. A case
6 of an intense anticyclonic eddy in the Balearic Sea (western Mediterranean), *J. Geophys. Res.*,
7 107(C11), 3183, doi:10.1029/2001JC000913.

8 Peltier, W. R., and R. Drummond, 2008. Rheological stratification of the lithosphere: A direct
9 inference based upon the geodetically observed pattern of the glacial isostatic adjustment of
10 the North American continent, *Geophys. Res. Lett.*, 35, L16314, doi:10.1029/2008GL034586.

11 Pettenuzzo, D., W. G. Large, and N. Pinardi, 2010. On the corrections of ERA-40 surface flux
12 products consistent with the Mediterranean heat and water budgets and the connection
13 between basin surface total heat flux and NAO, *J. Geophys. Res.*, 115, C06022,
14 doi:10.1029/2009JC005631.

15 Pinardi, N., Zavatarelli, M., Adani, M., Coppini, G., Fratianni, C., Oddo, P., Simoncelli, S.,
16 Tonani, M., Lyubartsev, V., Dobricic, S., Bonaduce, A., 2013. Mediterranean Sea large-scale
17 low-frequency ocean variability and water mass formation rates from 1987 to 2007: A
18 retrospective analysis. *Prog. Oceanogr.* (2013),
19 <http://dx.doi.org/10.1016/j.pocean.2013.11.003>.

20 Radu, R., Déqué, M. and S. Somot, 2008. Spectral nudging in a spectral regional climate
21 model. *Tellus A*, 60: 898–910. doi: 10.1111/j.1600-0870.2008.00341.x.

22 Reynolds, R. W., Smith, T. M., Liu, C., Chelton, D. B., Casey, K. S., and Schlax, M. G.,
23 2007. Daily high-resolution blended analyses for sea surface temperature, *J. Climate*, 20,
24 5473–5496.

25 Rio, M. H., Guinehut, S., and Larnicol, G., 2011. New CNES-CLS09 global mean dynamic
26 topography computed from the combination of GRACE data, altimetry, and in situ
27 measurements, *J. Geophys. Res.*, 116, C07018, doi:10.1029/2010JC006505.

28 Rixen, M., et al., 2005. The Western Mediterranean Deep Water : A proxy for climate change,
29 *Geophysical Research Letters*, 32(L12608), 1–4.

1 Robinson, A.R., Hecht, A., Pinardi, N., Bishop, J., Leslie, W.G., Rosentroub, Z., Mariano,
2 A.J., Brenner, S., 1987. Small synoptic/mesoscale eddies and energetic variability of the
3 eastern levantine basin. *Nature* 327 (6118), 131–134.
4 <http://dx.doi.org/http://dx.doi.org/10.1038/327131a0>.

5 Robinson, A. R., W. G. Leslie, A. Theocharis, and A. Laskaratos, 2001. Mediterranean Sea
6 circulation. *Encyclopedia of Ocean Sciences*, J. H. Steele, S. A. Thorpe, and K. K. Turekian,
7 Eds., Academic Press, 1689–1706.

8 Roether W., B. Klein, B. B. Manca, A. Theocharis, S. Kioroglou (2007) Transient Eastern
9 Mediterranean deep waters in response to the massive dense-water output of the Aegean Sea
10 in the 1990s , *Progress in Oceanography* 74 (2007) 540–571,
11 doi:10.1016/j.pocean.2007.03.001.

12 Rubio, A., B. Barnier, G. Jorda`, M. Espino, and P. Marsaleix (2009), Origin and dynamics of
13 mesoscale eddies in the Catalan Sea (NW Mediterranean): Insight from a numerical model
14 study, *J. Geophys. Res.*, 114, C06009, doi:10.1029/2007JC004245.

15 Ruti, P., S. Marullo, F. D’Ortenzio, M. Tremant, 2007. Comparison of analyzed and measured
16 wind speeds in the perspective of oceanic simulations over the Mediterranean basin:
17 Analyses, QuikSCAT and buoy data. *Journal of Marine Systems*, Vol. 70, Issues 1-2, P. 33-
18 48. doi:10.1016/j.jmarsys.2007.02.026.

19 Ruti PM, Somot S, Giorgi F, Dubois C, Flaounas E, Obermann A, Dell’Aquila A, Pisacane
20 G, Harzallah A, Lombardi E, Ahrens B, Akhtar N, Alias A, Arsouze T, Aznar R, Bastin S,
21 Bartholy J, Béranger K, Beuvier J, Bouffies-Cloch e S, Brauch J, Cabos W, Calmanti S,
22 Calvet J-C, Carillo A, Conte D, Coppola E, Djurdjevic V, Drobinski P, Elizalde-Arellano A,
23 Gaertner M, Gal an P, Gallardo C, Gualdi S, Goncalves M, Jorba O, Jord a G, L’Heveder B,
24 Lebeaupin-Brossier C, Li L, Liguori G, Lionello P, Maci as D, Nabat P, Onol B, Raikovic B,
25 Ramage K, Sevault F, Sannino G, MV Struglia, Sanna A, Torma C, Vervatis V., 2015. MED-
26 CORDEX initiative for Mediterranean Climate studies (BAMS, in revision).

27 Sanchez-Gomez, E., S. Somot, S. A. Josey, C. Dubois, N. Elguindi and M. D equ e, 2011.
28 Evaluation of Mediterranean Sea water and heat budgets simulated by an ensemble of high
29 resolution regional climate models. *Clim. Dyn.*, Vol. 37, Issue 9-10, pp 2067-2086.

1 Schroeder K., A. Ribotti, M. Borghini, R. Sorgente, A. Perilli, and G. P. Gasparini (2008) An
2 extensive western Mediterranean deep water renewal between 2004 and 2006 ,
3 GEOPHYSICAL RESEARCH LETTERS, VOL. 35, L18605, doi:10.1029/2008GL035146.

4 Sevault, F., S. Somot, A. Alias, C. Dubois, C. Lebeaupin-Brossier, P. Nabat, F. Adloff, M.
5 Déqué and B. Decharme, 2014. A fully coupled Mediterranean regional climate system
6 model : design and evaluation of the ocean component for the 1980-2012 period. *Tellus A*
7 2014, 66, 23967, <http://dx.doi.org/10.3402/tellusa.v66.23967>.

8 Solé J., Ruiz S., Pascual A., Somot S., Tintoré J. (2012) Ocean color response to wind forcing
9 in the Alboran Sea : a new forecasting method. *J. Mar. Syst.* Vol 98-99:1-8. Doi:
10 10.1016/j.jmarsys.2012.02.007.

11 Somot, S., F. Sevault, and M. Deque, 2006. Transient climate change scenario simulation of
12 the Mediterranean Sea for the twenty-first century using a high-resolution ocean circulation
13 model, *Climate Dynamics*, 27, 851–879.

14 Sorgente R, A. Olita, P. Oddo, L. Fazioli, A. Ribotti (2011) Numerical simulation and
15 decomposition of kinetic energy in the Central Mediterranean: insight on mesoscale
16 circulation and energy conversion , *Ocean Sci.*, 7, 503–519, 2011 , [www.ocean-](http://www.ocean-sci.net/7/503/2011/)
17 [sci.net/7/503/2011/](http://www.ocean-sci.net/7/503/2011/) , doi:10.5194/os-7-503-2011.

18 Sotillo, M. G., A. W. Ratsimandresy, J. C. Carretero, A. Bentamy, F. Valero, and F.
19 Gonzalez-Rouco, 2005. A high-resolution 44-year atmospheric hindcast for the
20 Mediterranean Basin : contribution to the regional improvement of global reanalysis, *Climate*
21 *Dynamics*, 25, 219–236.

22 Soto-Navarro, J., F. Criado-Aldeanueva, J. Garcia-Lafuente, and A. Sanchez-Roman, 2010.
23 Estimation of the Atlantic inflow through the Strait of Gibraltar from climatological and in
24 situ data, *Journal of Geophysical Research*, 115(C10023), doi :10.1029/2010JC006302.

25 Soto-Navarro, J., S. Somot, F. Sevault, J. Beuvier, F. Criado-Aldeanueva, J. Garcia-Lafuente
26 and K. Béranger, 2014. Evaluation of regional ocean circulation models for the Mediterranean
27 Sea at the Strait of Gibraltar: volume transport and thermohaline properties of the outflow.
28 *Clim. Dyn.* doi :10.1007/s00382-014-2179-4.

29 Stanev, E. V., and E. L. Peneva, 2002. Regional sea level response to global climatic change:
30 Black Sea examples, *Global Planet. Changes*, 32, 33–47.

1 Struglia, M.V., Mariotti, A., Filograsso, A., 2004. River discharge into the Mediterranean
2 Sea: climatology and aspects of the observed variability. *Journal of Climate* 17 (24), 4740–
3 4751. <http://dx.doi.org/10.1175/JCLI-3225.1>"<http://dx.doi.org/10.1175/JCLI-3225.1>.

4 Tonani, M., Pinardi, N., Dobricic, S., Pujol, I., and Fratianni, C.: A high-resolution free-
5 surface model of the Mediterranean Sea, *Ocean Sci.*, 4, 1-14, doi:10.5194/os-4-1-2008, 2008.

6 Vervatis, V. D., S. S. Sofianos, N. Skliris, S. Somot, A. Lascaratos, and M. Rixen (2013),
7 Mechanisms controlling the thermohaline circulation pattern variability in the Aegean-
8 Levantine region. A hindcast simulation (1960-2000) with an eddy resolving model, *Deep-*
9 *Sea Research Part I*, 74:82-97, doi:10.1016/j.dsr.2012.12.011

10 Vrac M., P. Drobinski, A.
11 Merlo, M. Herrmann, C. Lavaysse, L. Li, S. Somot, 2012. Dynamical and statistical
12 downscaling of the French Mediterranean climate: uncertainty assessment. *Natural Hazards*
13 and *Earth System Sciences*, European Geosciences Union, 2012, 12, pp.2769-2784.
<10.5194/nhess-12-2769-2012>

14 Wüst, G., 1961. On the vertical circulation of the Mediterranean Sea, *J. Geophys. Res.*,
15 66(10), 3261–3271, doi:10.1029/JZ066i010p03261.

16
17
18
19
20
21
22
23
24
25
26
27
28

1
2
3

Dataset	Shortwave	Longwave	Latent heat	Sensible heat	Net surface heat flux
Reference	[183 , 185]	[-84 , -75]	[-90 , -88]	[-14 , -6]	[-5 , -1]
ALDERA	204	-85	-112	-10	-3
ARPERA2	187	-79	-111	-12	-15
ERA-Int (1989-2004)	198	-83	-97	-12	+6
Pettenuzzo et al. 2010 (1958-2001)	180	-80	-91	-14	-5
ALADIN at 50km	196	-81	-111	-11	-7
ALADIN at 150km	200	-82	-94	-10	+14
ENSEMBLES RCMs	[154 , 214]	[-100 , -70]	[-128 , -85]	[-22 , -8]	[-40 , +21]

4

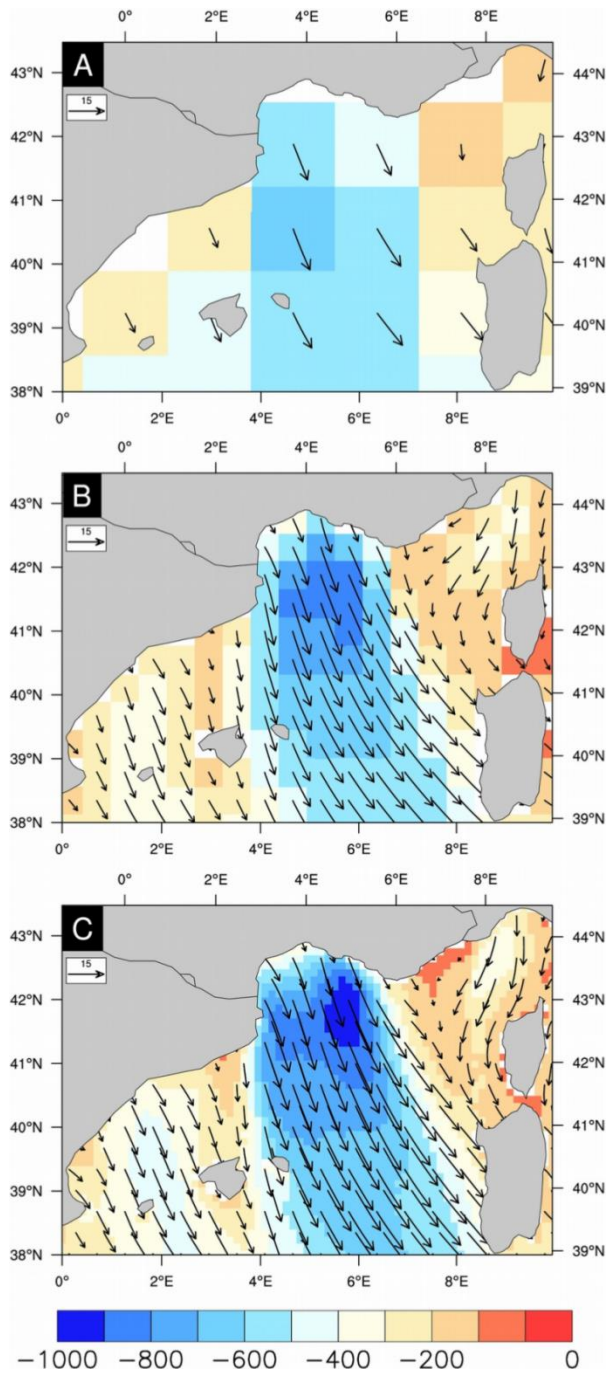
5 Table 1: Mediterranean Sea averaged and temporal averaged values of the various terms of
6 the sea surface heat budget (W/m²). Values are computed over the 1985-2004 period except
7 for when indicated. The reference comes from Sevault et al. (2014). The so-called
8 ENSEMBLES RCMs is an ensemble of 15 runs carried out with state-of-the-art RCMs during
9 the EU project ENSEMBLES at 25km, driven by the ERA-40 reanalysis over the 1958-2001
10 period (see Sanchez-Gomez et al. 2011).

1

Dataset	Evaporation	Precipitation	River runoff	Black Sea freshwater inputs	Net surface water flux
Reference 1	-3.1	0.7	0.4	0.3	-1.7
Reference 2	[-3.3 , -2.9]	[0.6 , 0.8]	[0.3 , 0.5]	[0.2 , 0.4]	[-2.0 , -1.4]
ALDERA (1979-2011)	-4.0	1.6	0.4*	0.3*	-1.7
ARPERA2 (1958-2008)	-3.9	1.8	0.2**	0.3**	-1.6**
ERA-Int (1989-2004)	-3.2	1.4	-	-	
Pettenuzzo et al. 2010 (1958-2001)	-3.2	1.4	-	-	
ALADIN at 50km (1979-2011)	-4.0	1.4	0.4*	0.3*	-1.9
ALADIN at 150km (1979-2011)	-3.3	1.1	0.4*	0.3*	-1.5
ENSEMBLES RCMs	[-4.4 , -2.9]	[1.0 , 1.7]	[0.2 , 0.6]	[0.1 , 0.5]	[-2.0 , -1.2]

2

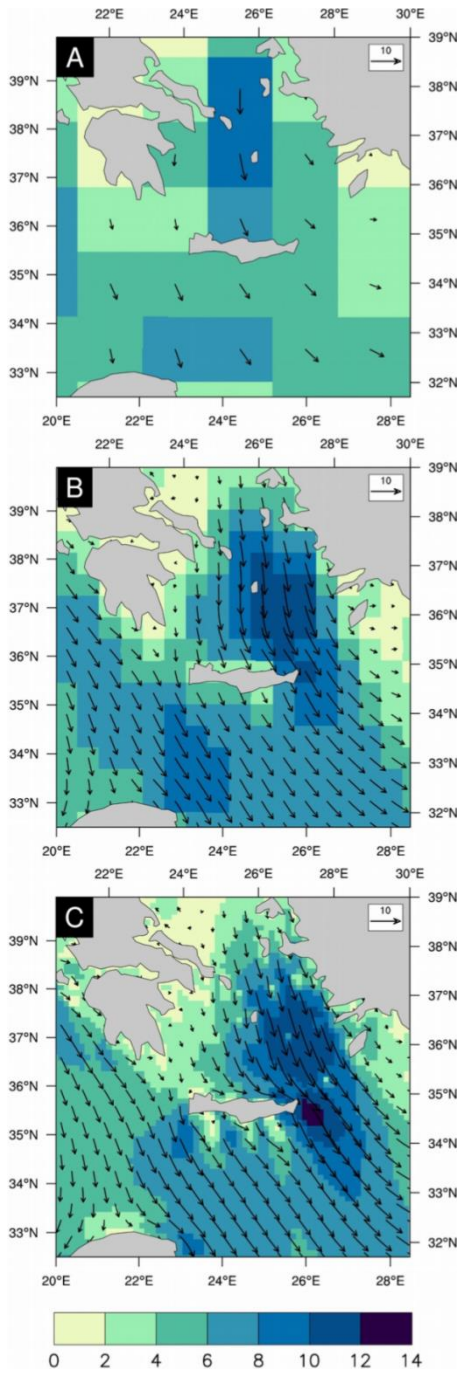
3 Table 2: Same as Table 1 but for the Mediterranean Sea surface water budget terms
4 (mm/day). The reference 1 comes from Sanchez-Gomez et al. (2011) and the reference 2 from
5 Dubois et al. (2010). The reference values do not always cover a common period. * : the
6 ALDERA atmospheric forcing is here completed by the river runoff and Black Sea freshwater
7 inputs coming respectively from Ludwig et al. (2009) and Stanev et al. (2008) as used in
8 Beuvier et al. (2012b) and in MEDRYS. ** : the ARPERA2 atmosphere forcing is here
9 completed by the river runoff and Black Sea freshwater inputs coming respectively from
10 Ludwig et al. (2009) and Stanev et al. (2008) as used in the Herrmann et al. (2010) paper.



1

2

3 Figure 1: Daily average wind direction (arrows) and latent heat flux (color in $W.m^{-2}$) on
 4 March 14th 2013 in (a) ALADIN-150km, (b) ALADIN-50km and (c) ALADIN-12km (the
 5 so-called ALDERA).



1

2

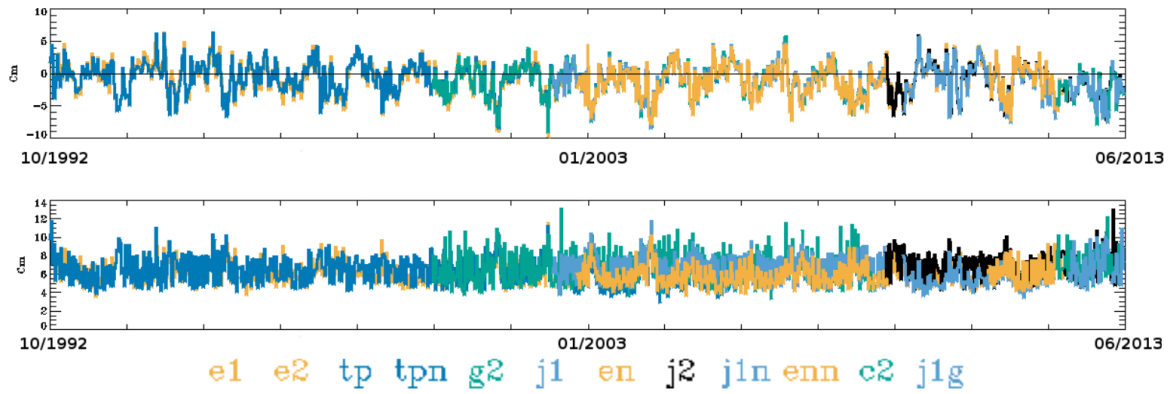
3 Figure 2: Daily average wind direction (arrows) and wind speed (color in m.s^{-1}) on August
 4 16th 2012 in (a) ALADIN-150km, (b) ALADIN-50km and (c) ALADIN-12km (the so-called
 5 ALDERA).

1

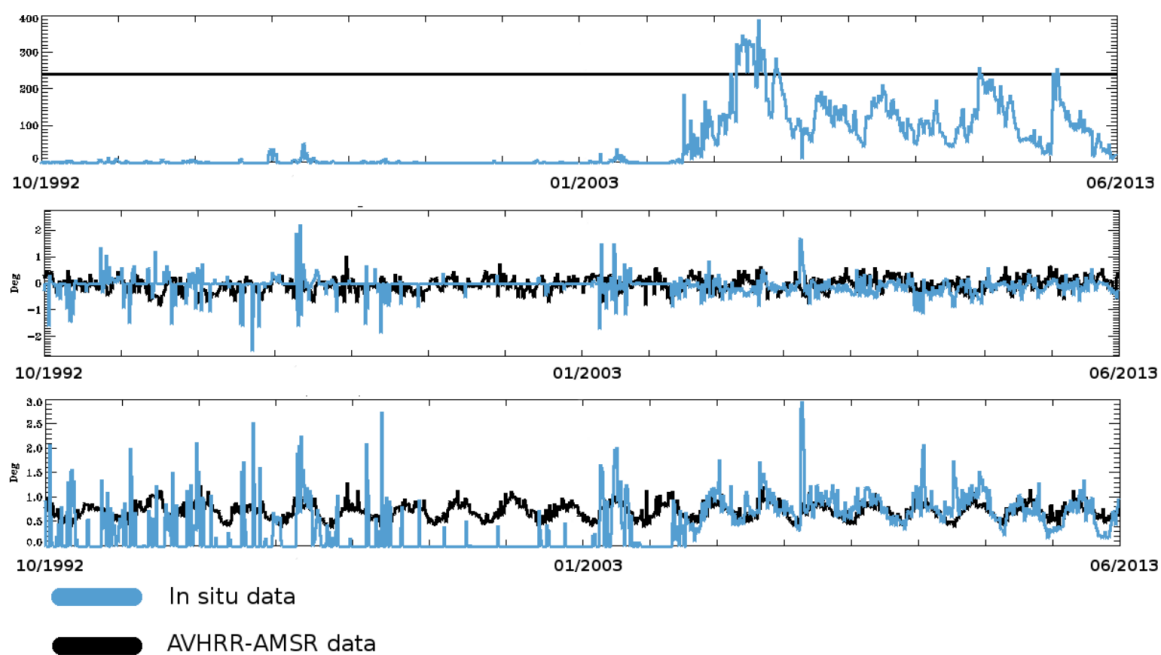
Satellite name	Acronym	Begin	End
ERS2	e2	15/05/1995	09/04/2003
Topex/Poseidon	tp	25/09/1992	24/04/2002
Topex/Poseidon (interleaved)	tpn	16/09/2002	08/10/2005
Geosat Follow-On	g2	07/01/2000	07/09/2008
Jason 1	j1	24/04/2002	19/10/2008
Envisat	en	09/10/2002	22/10/2010
Jason 2	j2	19/10/2008	now
Jason 1 (interleaved)	j1n	14/02/2009	now
Envisat (interleaved)	enn	22/10/2010	now
Cryosat 2	c2	19/02/2012	now
Jason 1 Geodetic	j1g	14/05/2012	now

2

3 Table 3: Name, acronym and period of SLA measurement for all satellite used by the
4 assimilation process.



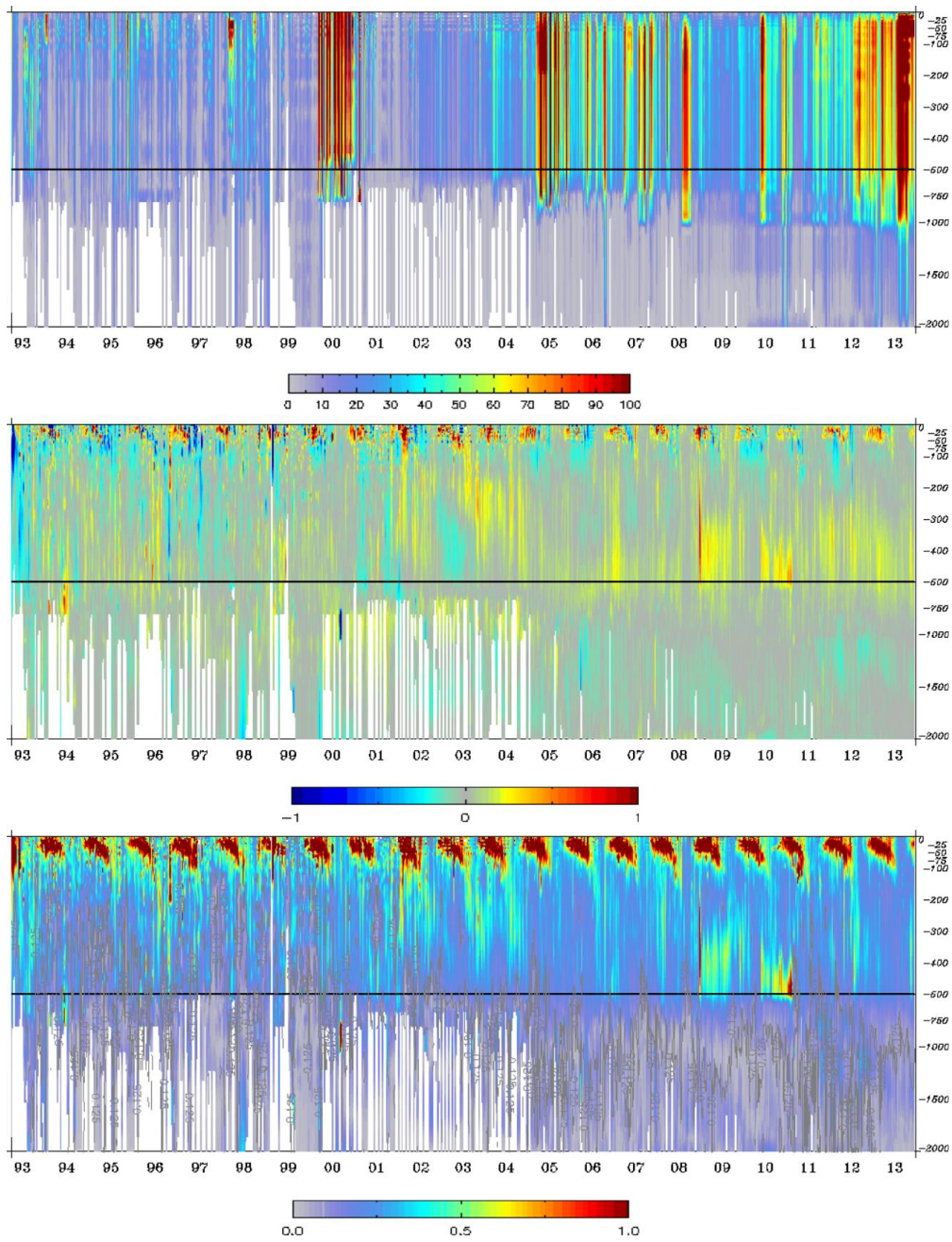
3 Figure 3: Time series of weekly sea level anomaly (SLA, m) data assimilation statistics
 4 averaged over the whole Mediterranean basin : mean innovation (top) and RMS of innovation
 5 (bottom). The colors stand for different satellites (please refer to Tab. 3).



1

2

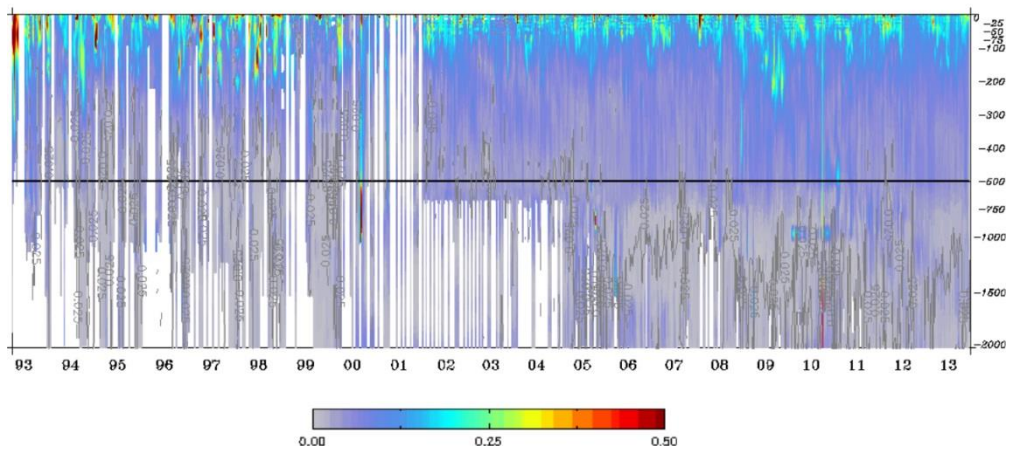
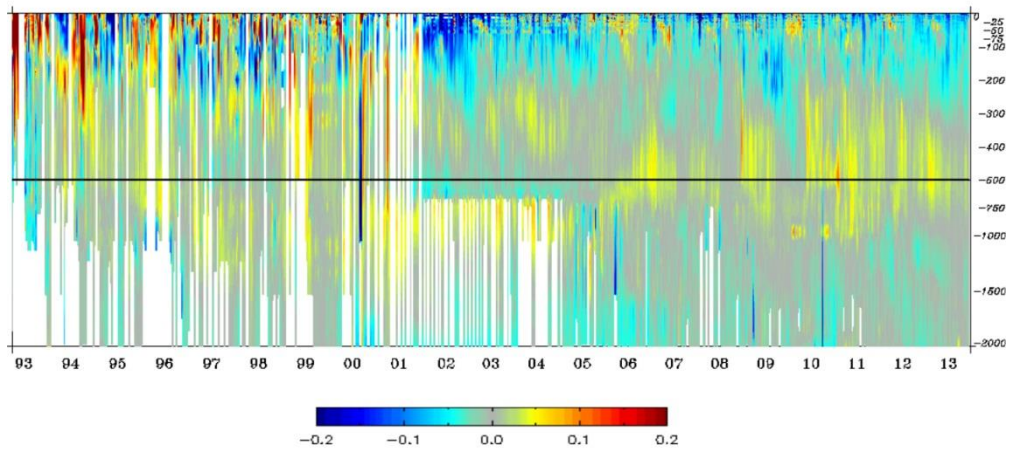
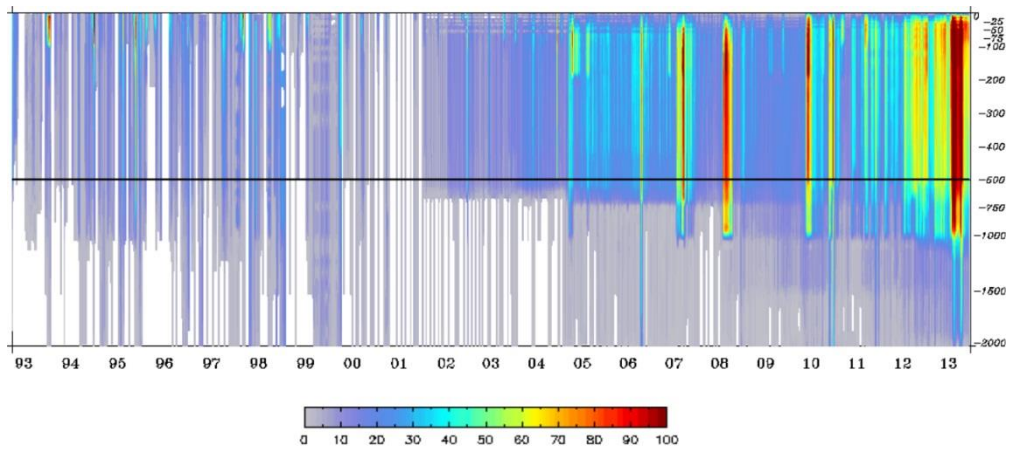
3 Figure 4: Time series of weekly sea surface temperature (SST, °C) data assimilation statistics
 4 from in situ (blue) and satellite SST AVHRR-AMS (black), averaged over the whole
 5 Mediterranean basin : number of data (top), mean innovation (middle) and RMS of innovation
 6 (bottom).



1

2

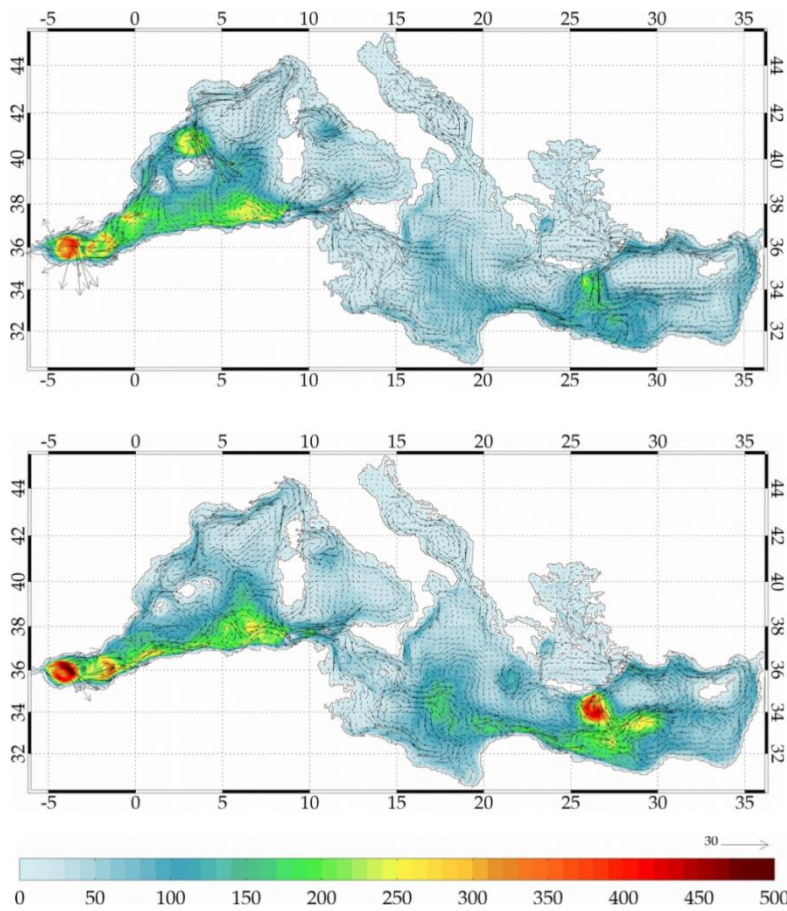
3 Figure 5: Evolution of weekly temperature data assimilation statistics from in situ profiles,
 4 function of the depth averaged over the whole Mediterranean basin : number of observations
 5 (top), mean innovation (middle) and RMS of the innovation (bottom).



1

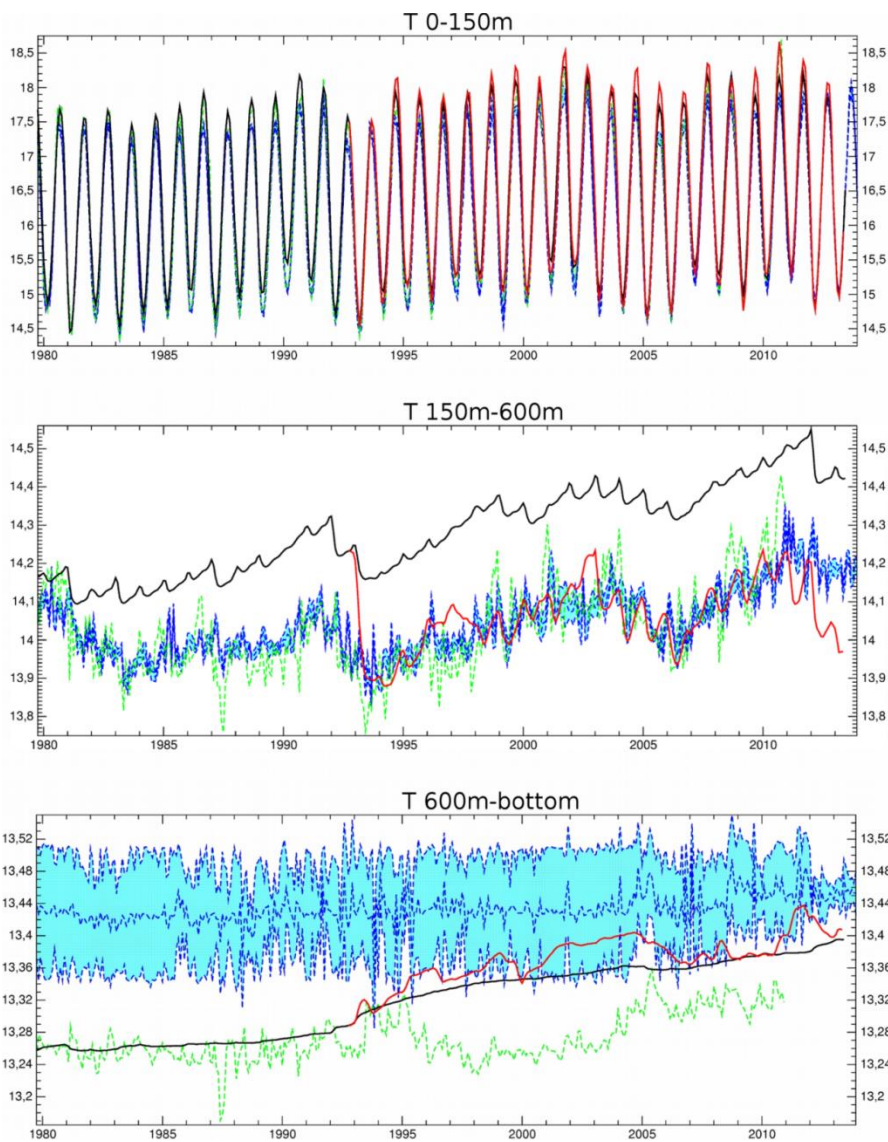
2

3 Figure 6: Evolution of weekly salinity data assimilation statistics from in situ profiles,
 4 function of the depth averaged over the whole Mediterranean basin : number of observations
 5 (top), mean innovation (middle) and RMS of the innovation (bottom).



1
2

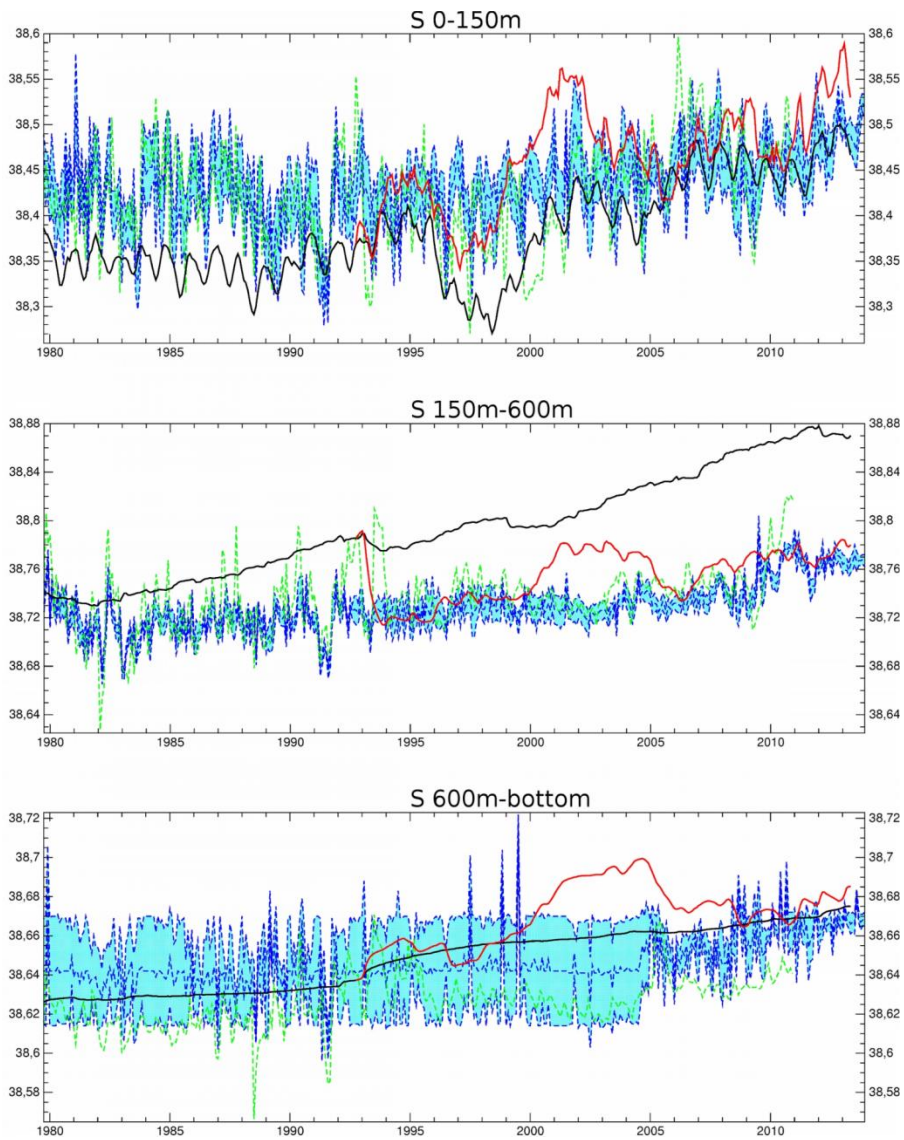
3 Figure 7: Mean Eddy Kinetic Energy (EKE in $\text{cm}^2 \cdot \text{s}^{-2}$) at 40m depth over the period 1992-
 4 2013 for NM12-FREE (top) and MEDRYS (bottom). Arrows represent the mean currents (in
 5 $\text{cm}^2 \cdot \text{s}^{-1}$) over the same period and at the same depth.



1

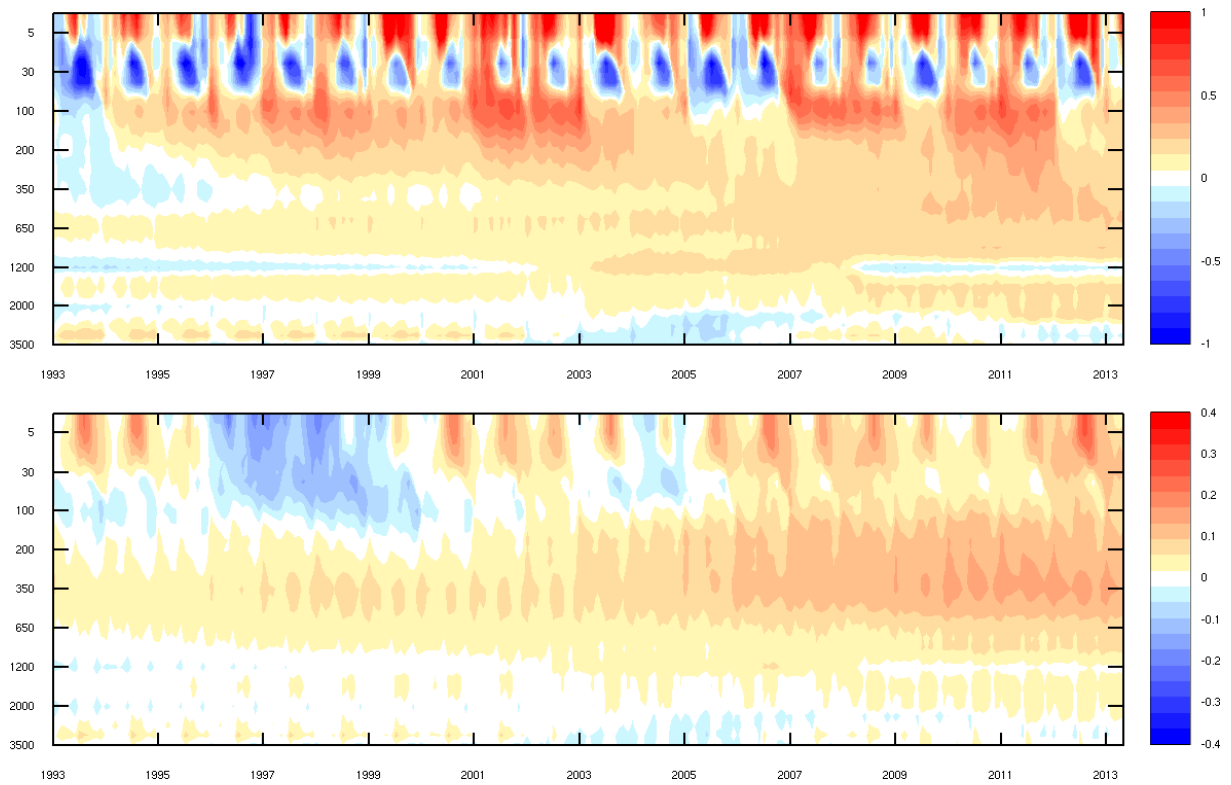
2

3 Figure 8: Evolution of the monthly integrated heat content (expressed as mean temperature
 4 in °C) over the Mediterranean basin for the layers 0m-150m (top), 150m-600m (middle) and
 5 600m-bottom (bottom) from MEDRYS (red line), NM12-FREE (black line), EN3 (dotted
 6 green line) and the IMEDEA (blue dotted line) hydrographic gridded products. The blue
 7 shaded area indicates the uncertainty ranges around the values of IMEDEA.



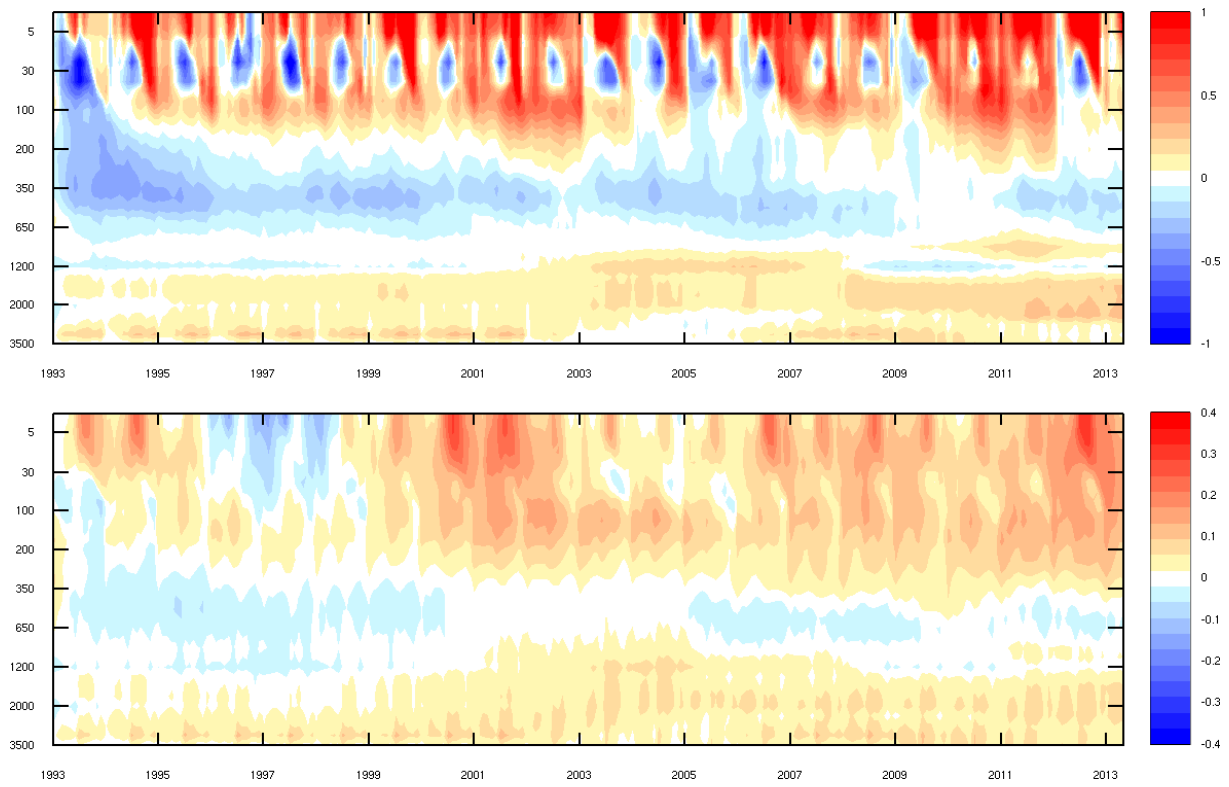
1
2
3
4

Figure 9: Same as Figure 8 but for integrated salt content (expressed as mean salinity in psu).



1
2

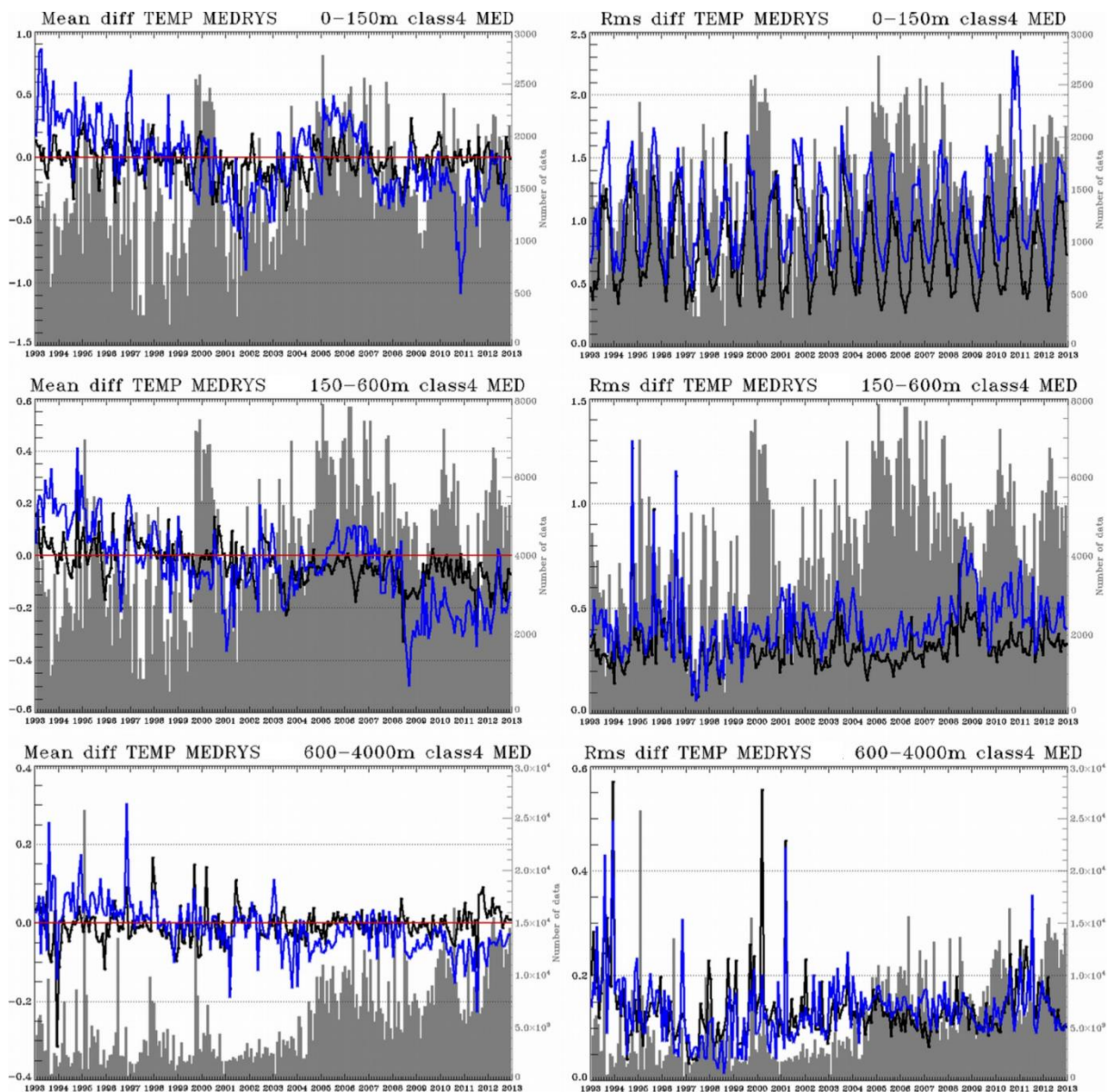
3 Figure 10: NM12-FREE basin mean temperature ($^{\circ}\text{C}$, above) and salinity (psu, below)
4 anomalies with respect to MedAtlas-1979.



1

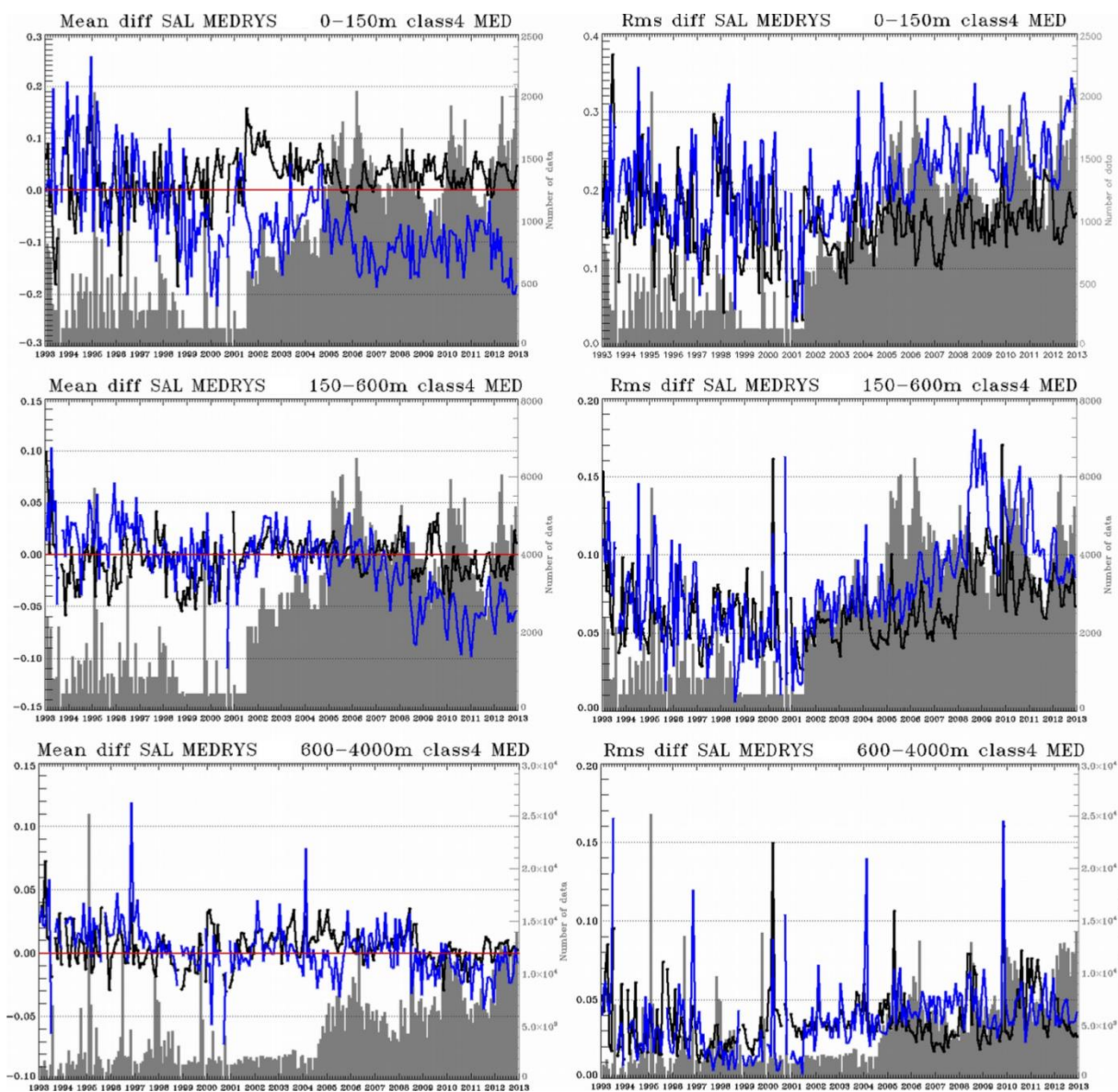
2

3 Figure 11: MEDRYYS basin mean temperature ($^{\circ}\text{C}$, above) and salinity (psu, below) anomalies
 4 with respect to MedAtlas-1979.



1
2

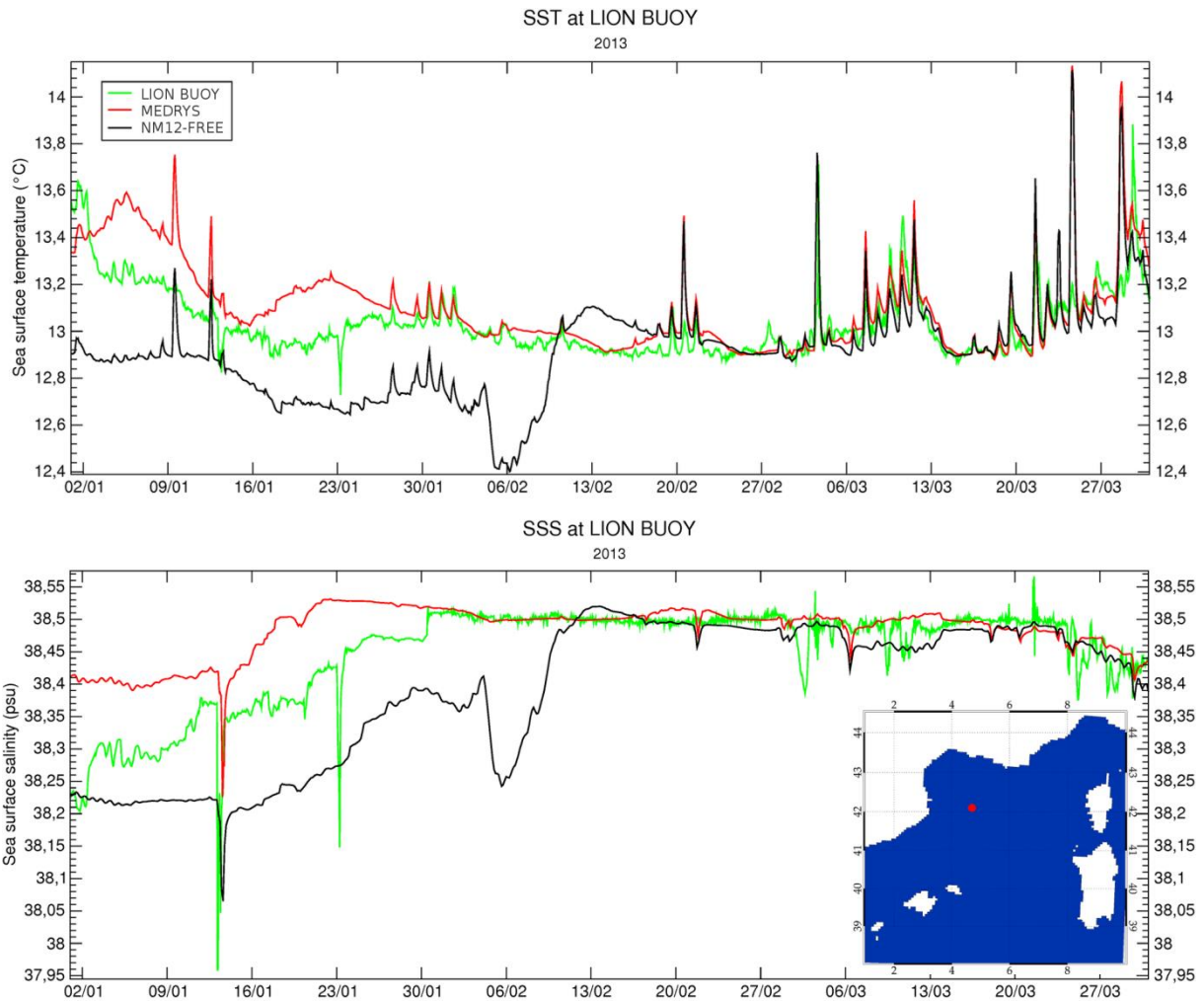
3 Figure 12: Temperature ($^{\circ}\text{C}$) mean (upper row) and RMS (bottom row) differences analysis
 4 minus observation (black), and MEDATLAS-1998 minus observation (blue). For these
 5 diagnostics, all available T/S observations from the CORIOLIS database and MEDRYS daily
 6 average analysis, collocated (temporally and spatially) with observations, are used. The
 7 number of observations is shown with gray bars. Averages are performed in the 0-150m (left),
 8 150-600m (middle) and 600m-4000m (right) layers in the whole Mediterranean basin.



1

2

3 Figure 13: Same as Fig. 12 but for salinity (psu).



1

2

3 Figure 14: Evolution of the hourly Sea Surface Temperature (SST, top) and Sea Surface
 4 Salinity (SSS, bottom) at the LION buoy location (red dot on the map) between 01/01/2013
 5 and 03/31/2013. The observation is shown with the green lines, NM12-FREE with the black
 6 lines and MEDRYS with the red lines.

	IN	OUT	NET
Water (<i>Sv</i>)			
NM12-FREE	+0.70 ± 0.03	-0.65 ± 0.03	+0.047 ± 0.009
MEDRYS	+0.81 ± 0.03	-0.77 ± 0.03	+0.048 ± 0.009
Heat (<i>W/m²</i>)			
NM12-FREE (averaged temperature)	+19.6 ± 0.9 17.18 °C	-14.1 ± 0.6 13.62 °C	+5.5 ± 0.4 (diff = +3.56 °C)
MEDRYS (averaged temperature)	+22.8 ± 0.9 17.13 °C	-16.2 ± 0.6 13.31 °C	+6.6 ± 0.4 (diff = +3.82 °C)
Salt (<i>10⁻³ psu/year</i>)			
NM12-FREE (averaged salinity)	+208 ± 8 36.49 psu	-205 ± 9 38.44 psu	+3.0 ± 2.6 (diff = -1.95 psu)
MEDRYS (averaged salinity)	+243 ± 9 36.54 psu	-241 ± 10 38.45 psu	+1.8 ± 2.8 (diff = -1.91 psu)

1

2

3 Figure 15: Average flow, heat and salt transport of the inflow and the outflow through the
4 Strait of Gibraltar at 5.5°W between 1992 and 2013 for NM12-FREE and MEDRYS. The
5 uncertainty corresponds to the annual standard deviation. For heat and salt transport, the
6 associated mean temperature and salinity in the layer are specified. The green color represents
7 values consistent with literature or/and reference products and the red color, those that are not
8 consistent.

9